Márcia Raquel Antunes Garcez
Licenciada em Bioquímica

The cellular basis of a congenital heart defect in *Drosophila*

Dissertação para obtenção do Grau de Mestre em
Bioquímica para a Saúde

Orientador: Doutor Alisson Gontijo, Investigador principal, CEDOC
Co-orientador: Doutora Fabiana Heredia, Investigadora associada, CEDOC

Setembro de 2015

Márcia Raquel Antunes Garcez
Licenciada em Bioquímica

The cellular basis of a congenital heart defect in *Drosophila*

Dissertação para obtenção do Grau de Mestre em
Bioquímica para a Saúde

Orientador: Doutor Alisson Gontijo, Investigador principal, CEDOC
Co-orientador: Doutora Fabiana Heredia, Investigadora associada, CEDOC

Setembro de 2015

Agradecimentos

Em primeiro lugar, uma grande palavra de agradecimento ao Alisson e à Fabiana por me terem dado a oportunidade de fazer parte do *Integrative Biomedicine Lab*. É difícil traduzir por palavras tudo o que aprendi durante este ano, que passou tão rápido. Obrigada por me terem dado a oportunidade de adquirir tantos novos conhecimentos científicos, e de aumentar o meu espirito critico intensificando a minha vontade de aprender mais e mais… Este foi sem dúvida um ano enriquecedor a nível pessoal, onde me superei e ultrapassei largamente as minhas espectativas. Obrigada por todo o tempo investido, pelo apoio, e pelo conhecimento transmitido. Espero não vos ter desiludido.

Aos meus colegas do *Integrative Biomedicine Lab*, por tornarem tão fácil todo o tempo e trabalho que partilhámos. Pela amizade, alegria e incentivo. Por me terem transmitido o melhor de cada um e me terem ajudado tantas vezes sem receberem nada em troca. Um especial obrigado ao André por toda a paciência, tempo e conhecimento que me ajudou infinitamente ao longo deste ano, à Andreia por sempre ter sido a ajuda necessária nos dias mais longos e à Maria João pela alegria súbita que instalou nesta fase final.

À Joana, ao Nuno e à Jéssica, pelo apoio e amizade. Obrigada pelo quentinho no coração ao saber que posso sempre contar com cada um de vós. Ao Filipe, por ouvir todos os meus lamentos, inseguranças e resmunguices. Porque mais do que ninguém sabes ver o melhor de mim. Obrigada pela força, confiança e calma que me transmites nas pequenas coisas. *When you're down and low, lower than the floor…*

À minha família, em especial aos meus tios, por me terem sempre ajudado, fazendo com que os últimos 5 anos fossem mais fáceis de superar. Obrigada pela companhia e conforto que minimizaram as saudades de casa. Aos meus avós por todo o carinho e preocupação. À minha irmã por todos os trabalhos de casa facilitados, pela paciência mutua para nos aturarmos e pelo apoio. Porque sinto que aconteça o que acontecer, temo-nos uma à outra.

Por último, e mais importante que tudo, os meus pais. Porque sem eles eu não poderia ser quem sou e muito menos estar onde estou. Sem o seu esforço, trabalho e apoio incondicional para que todas as decisões que eu tomei se tornassem em metas que consegui concretizar. O meu maior desejo é conseguir dar-vos em dobro tudo aquilo que até hoje me ofereceram sem pedir nada em troca. Obrigada por todo o esforço, carinho, dedicação e amor desmedido.

Abstract

Mutations in genes controlling heart development and abnormalities in any of its steps frequently cause cardiac malformations, the most common type of birth defects in humans, affecting nearly 1% of births per year. Hence around 20 million adults are expected to live with a congenital heart defect. The *Drosophila melanogaster* heart, called dorsal vessel, is a relatively simple organ that acts as a muscular pump contracting automatically to allow the circulation of hemolymph. *Drosophila* heart formation shares many similarities with heart development in vertebrates providing a powerful system to study gene networks and regulatory pathways involved in heart development. We have previously identified a *Drosophila* gene, *darhgef10*, which is strongly expressed in the developing heart and when deleted, leads to flies with highly prevalent yet subtle heart abnormalities, compatible with unchallenged life in the laboratory. Our aims were to phenotypically characterize homozygous null *darhgef10* mutants, characterize the subcellular localization of dArhgef10 and to study the cellular basis of the misaligned cardioblasts defect. We found that about half of *darhgef10* mutants die during development. However, the survivors surprisingly have a nearly normal developmental time, adult locomotor behavior and total lifespan. Detection of transgene-derived dArhgef10 protein *in vitro* and *in vivo* using custom antibodies revealed a cytosolic protein slightly enriched in the cellular membranes and associated with F-actin. Tissue-specific *darhgef10* expression disrupts the normal morphology of developing muscles, salivary glands and the eye. Live imaging of *darhgef10* mutant embryos revealed that heart defect could be caused by a reduced capacity of attachment of pericardial cells and/or alary muscle to dorsal vessel. The human homolog of *darhgef10* is also expressed in the heart and is a susceptibility gene for atherothrombotic stroke, suggesting that what we learn about the function of this gene and its phenotypes in *Drosophila* could have implications to human health.

Resumo

Mutações em genes envolvidos na formação do coração e anomalias em qualquer etapa deste processo causam frequentemente malformações cardíacas, que representam o tipo mais comum de defeitos em neonatais, afetando cerca de 1% dos nascimentos por ano. Assim, estima-se que 20 milhões de pessoas sejam portadoras de um defeito cardíaco congénito.

O coração da *Drosophila melanogaster* (mosca-da-fruta), denominado vaso dorsal, é um órgão relativamente simples que actua como uma bomba muscular, contraindo automaticamente para permitir a circulação da hemolinfa através do corpo. A formação do vaso dorsal na mosca é muito semelhante ao desenvolvimento do coração em vertebrados, representando por isso, um poderoso modelo para estudar a rede de genes e os padrões regulatórios relacionados com o desenvolvimento deste órgão. Anteriormente, nós identificámos um gene em *Drosophila*, *darhgef10*, fortemente expresso no coração em desenvolvimento e cuja deleção induz anormalidades cardíacas subtis mas prevalentes. Os mutantes para *darhgef10* são viáveis e férteis no ambiente controlado de laboratório.

Este trabalho teve como objectivos caracterizar fenotipicamente os mutantes nulos para *darhgef10*, determinar a localização subcelular da proteína dArhgef10 e investigar a base celular subjacente ao defeito no alinhamento dos cardioblastos observado nos mutantes. Os nossos resultados revelaram que a deleção de d*arhgef10* provoca uma severa redução da viabilidade, sem no entanto comprometer o tempo de desenvolvimento e a longevidade. Por outro lado, o aumento da expressão de *darhgef10* em músculos, glândulas salivares e no disco imaginal do olho afeta drasticamente a integridade destes tecidos. A expressão ectópica de *darhgef10 in vitro* e *in vivo* revelou que a proteína está localiza no citoplasma com enriquecimento junto à membrana celular, com associação à actina F. *Live imaging* de embriões mutantes para *darhgef10* revelou que os defeitos observados no coração podem estar associados a um defeito na adesão dos músculos *alary* e/ou das células pericardiais ao vaso dorsal. O homólogo humano de *darhgef10*, *ARHGEF10*, também é expresso no coração e está associação a uma maior susceptibilidade para a ocorrência de acidentes vasculares cerebrais

aterotrombóticos, sugerindo que o que aprendemos sobre *darhgef10* em *Drosophila* pode ter implicações do ponto de vista clínico para a saúde humana.

Index

List of tables

List of figures

List of abbreviations

aa	Aminoacid
AAE	After adult eclosion
Act	Actin
AEL	After egg laying
ANOVA	Analysis of variance
Arm	Armadillo
BDSC	Bloomington Drosophila Stock Center.
BLAST	Basic Local Alignment Search Tool
bp	Base pairs
BSA	Bovine serum albumin
Cas9	CRISPR associated protein 9
Cdc42	Cell division cycle 42
CG	Computed gene
CHD	Congenital heart diseases
chiRNA	Chimeric RNA
CMT	Charcot-Marie-Tooth
CRISPR	Clustered regularly interspaced short palindromic repeats
DAPI	4',6-diamidino-2-phenylindole
d*arhgef10*	Drosophila rho guanine nucleotide exchange factor 10
Df	Deficiency chromosome
DH	Dbl homology
dH_20	Destilated Water
DHR	Dock homology region
Dia	Diaphanous
DNA	Deoxyribonucleic acid
dNTPs	Deoxynucleotide
DOCK	Dedicator of cytokinesis
Dpp	Decapentaplegic
DSHB	Developmental Studies Hybridoma Bank
EDTA	Ethylenediaminetetraacetic acid

ERM	Ezrin, radixin, moesin
Ey	Eyeless
FBS	Fetal Bovine Serum
FGF	Fibroblasts growth factor
FLP	Flippase
FRT	Flippase recognition target
gDNA	genomic DNA
GDP	Guanosine diphosphate
GFP	Green fluorescent protein
gRNA	Guide Ribonucleic Acid
GTP	Guanosine triphosphate
H_2O	Water
HCl	Chloridric ácid
Hh	Hedgehod
HRP	Horseradish peroxidase
HSD	Honest significant difference
Kb	Kilo bases
kDa	kilo daltons
L1	First instar
L2	Second instar
L3	Third instar
Lam A	Laminin A
LIMK	LIM kinase
Mef2	Myocyte enhancer factor-2
Mg^{2+}	Magnesium
MLC	Myosin light chain
MM	Molecular marker
MRCK	Myotonic dystrophy kinase related cdc42-binding kinase
MYPT	Myosin light chain phosphatase
NaCl	Sodium chloride
O.N.	Overnight
OLLAS	E.coli OmpF Linker and mouse Langerin fusion Sequence

PAK	P21-activated kinases
PAM	Protospacer adjacent motif
PBAs	Polyclonal antibodies
PBS	Phosphate-buffered saline
PBST	Phosphate-buffered saline with Triton-X
PBSTw	Phosphate-buffered saline with Tween20
PCR	Polymerase Chain Reaction
PFA	Parafolmaldehyde
PH	Pleckstrin homology
Prc	Pericardin
PS	Penincilin-Streptomycin
qRT-PCR	Quantitative reverse transcription polymerase chain reaction
Rho	Ras family member
RhoGAPs	RhoGTPase-activating proteins
RhoGDI	Rho guanine nucleotide dissociation inhibitor
RhoGEFs	Rho guanine nucleotide exchange factors
RNA	Ribonucleic Acid
RNAi	RNA Interference
Robo	Roundabout
ROCK	Rho-associated protein kinase
RT	Room temperature
S2	Schneider's Drosophila Line 2 cells
SD	**S**tandard deviation
SDS	Sodium dodecyl sulfate
SDS-PAGE	Sodium dodecyl sulfate polyacrylamide gel electrophoresis
SEM	Standard error of the mean
sfGFP	Super folder Green fluorescence protein
sgRNA	Single guide RNA
SM-RFP	Somatic muscle red fluorescent protein
SNP	**S**ingle nucleotide polymorphism
SP1	Specificity protein 1
Svp	Seven-up

TAE	Tris-acetate
Tin	Tinman
Tris-HCL	Tris hydrochloride
Tub	Tubulin promoter
UAS	Upstream activating sequence
VRDC	Vienna Drosophila RNAi Center
W[1118]	White
WASP	Wiskott-Aldrich Syndrome Protein
Wg	Wingless

Chapter 1. Introduction

1.1 Congenital heart disease

Congenital heart diseases (CHD) define a group of structural and functional defects that arise during cardiac embryogenesis. These pathologies are the most common developmental birth defects, affecting about 1% of births per year worldwide. Epidemiologic studies suggest that genetic factors are the main cause of CHD (Fahed *et al.*, 2013; Gelb and Chung, 2014; Hoffman and Kaplan, 2002). However, the genetic mechanisms of heart development continue to be poorly understood and CHD are a significant cause of infant mortality and can result in chronic disability and increased medical treatment costs (Reller *et al.*, 2008). For instance, it is estimated that about 40 million adults live with a congenital heart defect in the world (this estimate is based on US adult CHD estimates and 2011 worldwide adult population estimates: J.I.E., 2013; Marelli *et al.*, 2007; Central Intelligence Agency 2011, The World Factbook 2011, ISSN 1553-8133, Washington, DC, viewed 17th April, 2011). These patients with this chronic illness are in increased risk of several complications such as infective endocarditis and hemodynamic decompensation, and can face life-threatening problems during contraception and pregnancy, with cardiac disease being one of the most common causes of indirect maternal death during pregnancy.

1.2 Heart development in *Drosophila*

Heart formation is a critical developmental process, tightly regulated in a sequential manner by multiple signaling pathways. Gene mutations and consequently deregulation of these pathways could lead to defective morphology and function of the mature heart, compromising the adult organism.

Many genes controlling early steps of heart development are highly conserved between vertebrates and invertebrates. *Drosophila* has a cardiac organ, called dorsal vessel or cardiac tube that constitutes the entire cardiovascular system of the organism and acts as a muscular pump contracting automatically to distribute the hemolymph through the body. Dorsal vessel formation shares many similarities with heart

development in vertebrates providing a powerful system to study gene networks and regulatory pathways involved in heart development (Wu and Luo, 2006).

The mature dorsal vessel is formed by two major cell types: the inner contractile cardioblasts which form the lumen of the heart and the non-muscular pericardial cells which forms the outer cell layers. The pericardial cells are thought to function in detoxification of the hemolymph (Bryantsev and Cripps, 2009; Vogler and Bodmer, 2015; Zhang *et al.*, 2013). The dorsal vessel is divided in two distinct parts: the aorta and the heart proper (Figure 1).

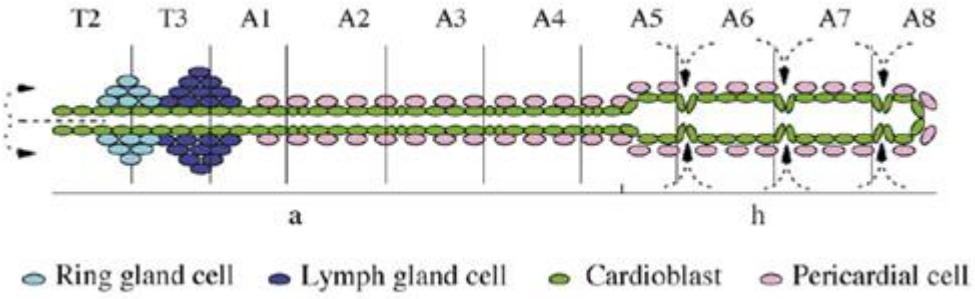

Figure 1 - Organization of embryonic dorsal vessel. The dorsal vessel can be divided in the heart region (h), posteriorly, and in the aorta region, anteriorly. The heart proper contains inflow tracts termed ostia cells. Dashed arrows show the hemolymph flow. Adapted from (Tao and Schulz, 2007).

The anterior region of the tube is surrounded by two glands: the endocrine ring gland and the hematopoietic lymph gland (Bier and Bodmer, 2004; Medioni *et al.*, 2009; Tao and Schulz, 2007). The heart is located at the posterior abdominal segments and contains inflow tracts, the ostium cells that open and close enabling entering of the hemolymph. This region, the only that shows automatically and synchronized beating, ends with a group of four cells that contribute to the major pacemaker activity of the organ. The aorta region, located anteriorly, is composed of a narrow lumen and ends in the outflow tracts. The cardiac tube is segmentally patterned, with mainly six pairs of cardioblasts per segment with a distinct genetic nature: four pairs have large nuclei and two have smaller nuclei (Medioni *et al.*, 2009; Tao and Schulz, 2007) (Figure 1).

As in vertebrates, the *Drosophila* dorsal vessel arises from the mesoderm (Figure 2) being specified through similar cellular induction pathways and transcription factors (Bodmer and Venkatesh, 1998; Cripps and Olson, 2002; Zaffran and Frasch, 2002). Upon Fibroblast growth factor (FGF) signaling, mesodermal cells invaginates and spread laterally forming a layer within the embryo (Mason, 1994). In the next stage, cells of the spreading mesoderm are specified as dorsal mesoderm by Decapentaplegic (Dpp) signaling. However, Dpp signaling is not sufficient to promote cardiac fate, thus ectodermally-derived signaling molecule Wingless (Wg) is required for the development of further specialized heart precursors (Wu, Golden and Bodmer, 1995). At this stage, Notch (N) signaling is essential for distinct cardiac progenitors leading to the formation of cardioblasts and pericardial cells (Han and Bodmer, 2003). The bilateral rows of aligned cardioblasts start to migrate dorsally and meet at the dorsal midline. In order to form a functional heart, Hedgehod (Hh) signaling molecule is secreted by the ectoderm and cardioblasts start specific differentiation programs. Due to Hh signaling, cardioblasts give rise to a sub-type of cardioblasts: cells with large nuclei (Tinman-positive cells) and cells with small nuclei (Svp/Doc-positive cells). Svp (COUP-TFII class protein Seven-up) is expressed in the anterior two pairs of cardioblasts in each segment of the dorsal vessel, which differentiate into three pairs of inflow tracts, ostia cells, in the heart proper region (Molina and Cripps, 2001; Park *et al.*, 1996; Ponzielli *et al.*, 2002). Tinman is responsible for the contractility of the four pairs of cardioblasts in the posterior region, making these cells adopt a contractile fate instead of the ostia cell fate (Zaffran *et al.*, 2006).

In addition to all transcription factors and signaling pathways involved in cardiac cell specification, many other genes and proteins are required for proper cardioblast alignment, migration and polarization. After specification of cardioblasts, the correct formation of the cardiac lumen is dependent on the correct polarity of cardiac cells, which is achieved by a dynamic control of cell shape changes and formation of membrane domains. In migrating cardiac cells, three distinct membrane domains can be specified due to specific cell polarity markers: L(luminal)-domain, J(junction)-domain and P(pericardin) A(adhesion)-domain. The L-domain faces the lumen of the tube. The J-domain forms adherent junctions between cardiac cells of opposite rows. The PA-

domain is the one that makes contacts between cardiac and pericardial cells (Medioni *et al.*, 2009; Tao and Schulz, 2007; Vogler and Bodmer, 2015) (Figure 3).

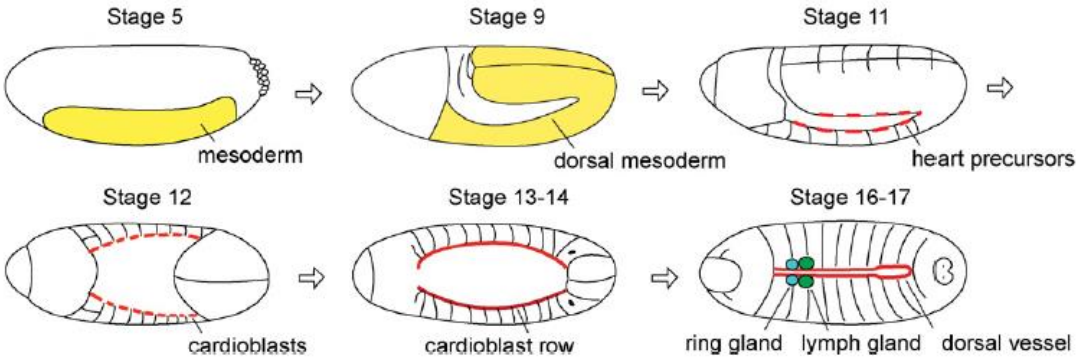

Figure 2 - Cardiogenesis in the *Drosophila* embryo. Dorsal vessel formation starts with mesoderm differentiation and after several specification events of heart precursors, the mature dorsal vessel is complete and functional in the stage 17. Adapted from (Tao and Schulz, 2007).

Specification and maintenance of such domains is assured by several regulators like the Slit/Robo pathway, which is required for specification of non-adherent/repulsive L-domains, DE-cadherin that establish adherent junctions and G_o proteins, members of the G protein family. These are responsible for the specification of the PA domains and the localization of proteins to these membrane domains to ensure proper cardioblast and pericardial cell adhesion. At the same time that the cardioblasts migrate to the dorsal midline, the leading edge cells interact with the adjacent ectoderm layer, which is in a coincident migration towards the midline in a process called dorsal closure. These interactions contribute to the movement of the cardioblasts. Such coordinated migration between the dorsal ectoderm and the associated cardioblasts rows also requires pericardin (prc), a component of the extracellular matrix that is produced by pericardial cells (Medioni *et al.*, 2009; Tao and Schulz, 2007) (Figure 3).

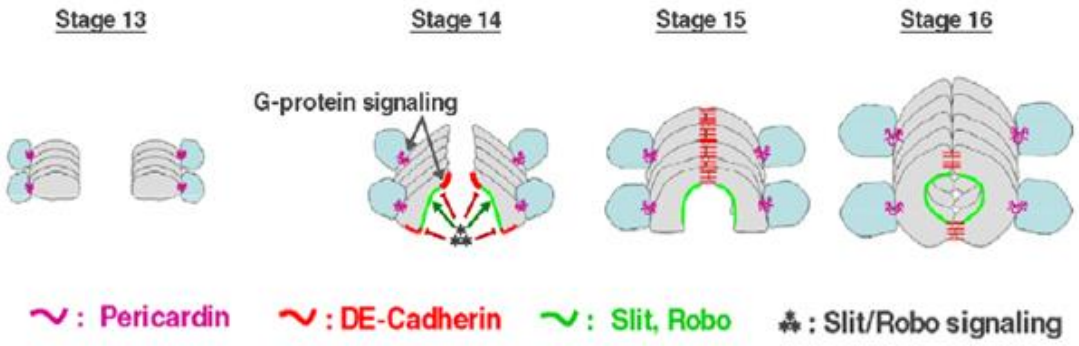

Figure 3 – Dorsal vessel formation during embryonic development. The cardioblast rows migrate towards the dorsal midline of the embryo. At stage 15, cardioblasts of opposite rows start to adhere at their edges to form the cardiac tube. Several proteins and signaling pathways are involved in the achievement and maintenance of the three different membrane domains that mediate tube formation (see text). Adapted from (Medioni *et al.*, 2009).

In the end of embryogenesis (stage 17), the mature dorsal vessel starts to beat as a functional cardiac organ. In the following larval stages, the cardiovascular system cells increase in size between 200-500 fold, maintaining their cellular identities. The adult heart is formed during metamorphosis by the remodeling of differentiated and already functional larval cardiomyocytes, without cell proliferation or addition of new cells (Hartenstein *et al.*, 1992; Park, Venkatesh and Bodmer, 1998).

1.3 Rho-family GTPases

Rho GTPases are a group of evolutionarily conserved proteins that function as intracellular transducers establishing a link between the cell surface signals and multiple intracellular responses, controlling a variety of cellular signal transduction pathways (Etienne-Manneville and Hall, 2002; Murali and Rajalingam, 2014; Ridley, 2001). These proteins belong to a main branch of the Ras superfamily of small GTPases and are ubiquitously expressed in all eukaryotic cells regulating many cellular events like actin cytoskeleton, cell-cycle progression, vesicle trafficking and gene transcription,

having an important role in cell adhesion, migration and polarity, neurite extension and retraction (Rossman, Der and Sondek, 2005; Sit and Manser, 2011).

RhoGTPases cycle between two conformational states: one GDP-bound state, and the other GTP-bound state. The GTP-bound state is able to interact and activate downstream effector proteins (Sit and Manser, 2011). Since RhoGTPases have the ability to regulate a wide variety of functions in very dynamic cellular context, they need to be tightly regulated. This regulation is achieved by three sets of proteins: Rho guanine nucleotide exchange factors (RhoGEFs), Rho GTPase activating proteins (RhoGAPs) and Rho guanine nucleotide dissociation inhibitors (RhoGDIs) (Heasman and Ridley, 2008) (Figure 4).

RhoGEFs activate RhoGTPases by catalyzing the release of GDP and the binding of GTP. In turn, RhoGAPs inactivate the proteins by enhancing the intrinsic GTPase activity to hydrolyze GTP to GDP. In order to retain the RhoGTPases in their inactive conformation, RhoGDIs bind to C-terminal prenyl groups sequestering them in the cytosol, preventing nucleotide exchange and membrane association. Altogether these proteins upregulate or downregulate the levels of membrane bound Rho proteins enabling thereby their spatio-temporal regulation (Heasman and Ridley, 2008; Pertz, 2010). Apart from these regulator proteins, RhoGTPases can also be regulated by post-translational modifications like phosphorylation and ubiquitination. Ubiquitin-dependent regulation can affect the stability of these proteins and for instance influence the plasticity of cell migration (Ekenstedt *et al.*, 2014; Murali and Rajalingam, 2014; Pareyson, 1999).

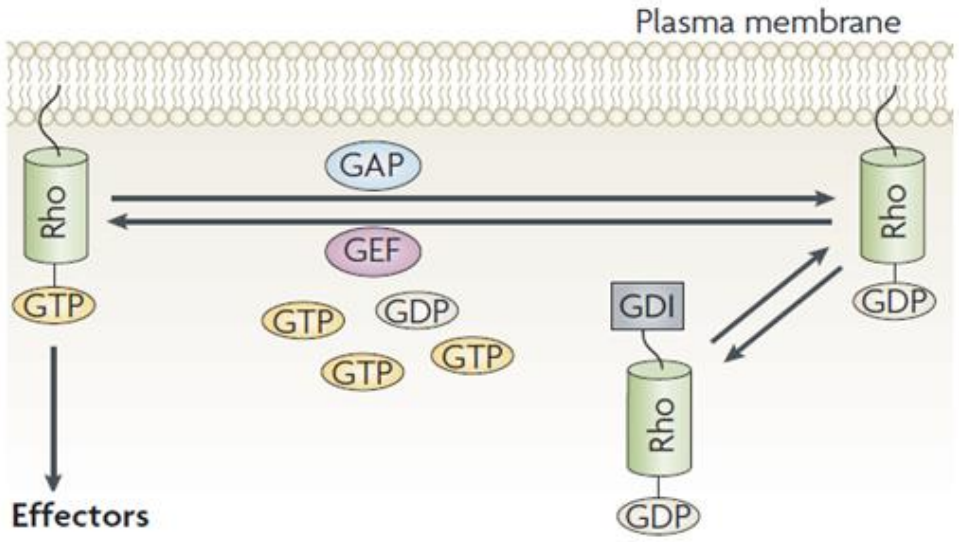

Figure 4 - Regulation of RhoGTPases by RhoGAP, RhoGEF and RhoGDI. When active, in the GTP bound state, RhoGTPases can interact with downstream effector proteins, regulating many cellular responses. Adapted from (Heasman and Ridley, 2008).

Until now, about 20 members of Rho GTPases have been identified in humans. Of these, RhoA, Rac1 and Cdc42 are the main and best studied groups. Over 70 GAPs and 80 GEFs have been identified, most of them showing tissue specific expression. The *Drosophila* genome encodes for seven Rho family members including the human homologs of Rho1, Rac1 and Cdc42 (Schmidt and Hall, 2002). The high number of functions for RhoGTPases is consistent with their large list of target proteins. This includes serine/threonine kinases, tyrosine kinases, lipases and scaffold proteins (Bishop and Hall, 2000). Despite all the functions described, RhoGTPases are best known for their function as regulators of the actin cytoskeleton and cell migration. Thus, the best studied effectors are proteins that interact with Rac1, RhoA and cdc42, which were discovered mainly for their influence in cell shape and plasticity of cell migration (Murali and Rajalingam, 2014; Sadok and Marshall, 2014).

Cell migration is a dynamic process that needs to be precisely regulated in order to allow continuous remodeling of the cellular architecture. This reorganization of the actin cytoskeleton enables the cell to move and adapt to changes in the surrounding

environment (Sadok and Marshall, 2014). In figure 5, a cell migration event is depicted: highly dynamic lamellipodia and filopodia are extended at the leading edge, containing actin filaments; cell translocation occurs through actomyosin-based contraction forces; retraction fibers pull the rear of the cell forward (Mattila and Lappalainen, 2008).

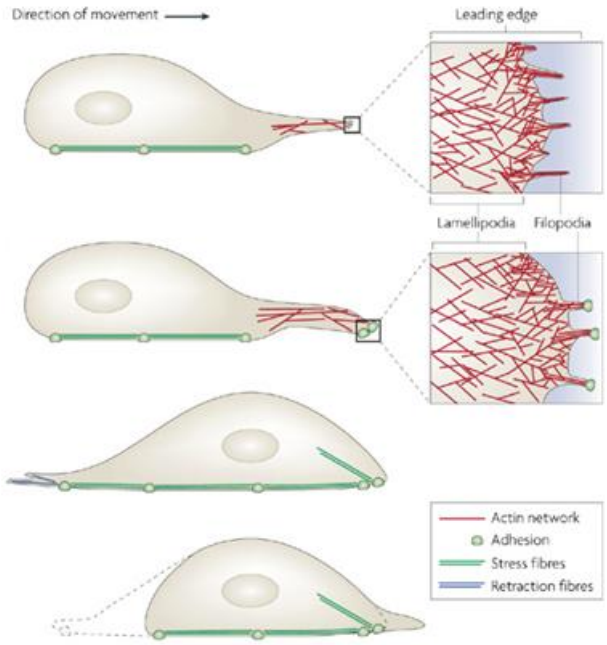

Figure 5 - Cell migration. Adapted from (Mattila and Lappalainen, 2008).

Altogether, Rac1, RhoA and Cdc42 promote a set of events that lead to new and/or reorganized actin filaments (Figure 6). Rac activates the Arp 2/3 complex through WAVE, leading to actin polymerization and lamellipodia formation. Additionally, it activates the serine/threonine kinase PAK that phosphorylates LIM kinase (LIMK), which inhibits cofilin, an actin binding protein that regulates the assembly and disassembly of actin filaments, thereby regulating actin-filament turnover. In turn, Rho activates ROCK which inactivates the myosin light chain phosphatase (MYPT) and consequently activates myosin II. Actomyosin contractility can also be promoted by Cdc42 via MRCK (myotonic dystrophy kinase related cdc42-binding kinase) because it also inactivates MYPT. Cdc42 contributes to filopodia extension through WASP and PAK, connecting with Rac and Rho. mDia (Diaphanous), a formin

protein, seems to be a common effector, leading to actin polymerization (Heasman and Ridley, 2008; Murali and Rajalingam, 2014) (Figure 6).

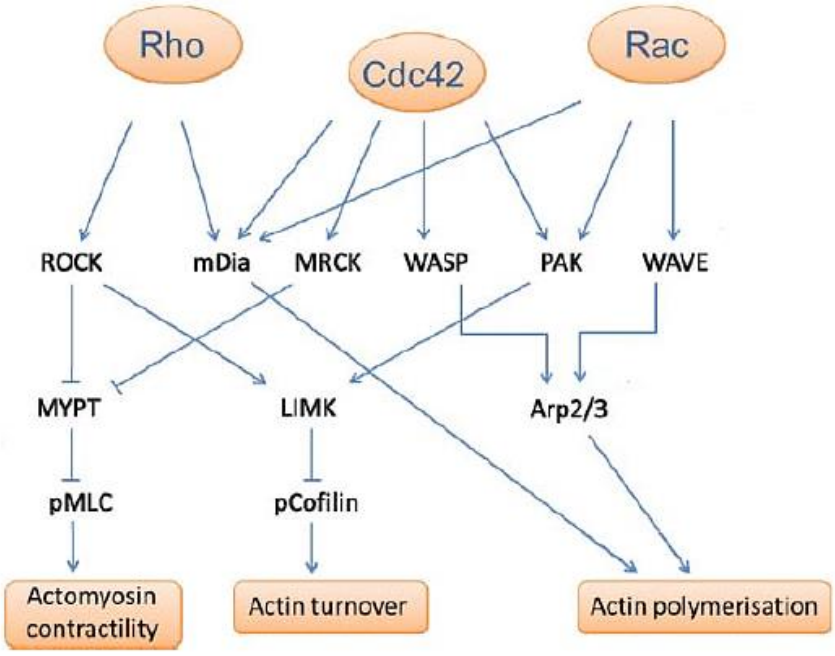

Figure 6 - RhoA, Rac1 and cdc42 and their effectors proteins in cell migration. Adapted from (Sadok and Marshall, 2014).

In a simplistic way, we can summarize that Rac1 mainly regulates membrane protrusions at the leading edge, Cdc42 controls filopodia formation and cell polymerization and RhoA controls contractility at the back of the cell. Nevertheless, this is a too simple 2D model and new results have showed a more complex organization highly regulated. More and more, fluorescent probes are used to report RhoGTPase signaling in time and space, giving new insights to our knowledge in this not so simple concept (Pertz, 2010).

1.4 Rho guanine nucleotide exchange factors

Since RhoGTPases play a prominent role in many aspects of cell biology, they need to be tightly regulated. Along with the regulatory factors RhoGAP and RhoGDI, RhoGEFs provides fine control over the signaling events mediated by RhoGTPases (Cherfils and Zeghouf, 2013). RhoGEFs catalyze the displacement of the bound GDP and subsequent exchange with cytosolic GTP, generating the active form of RhoGTP that is capable of recognizing a wide variety of effector proteins (Bishop and Hall, 2000; Etienne-Manneville and Hall, 2002).

In the human genome RhoGEFs are encoded by two unrelated gene families, Dbl and DOCK, in a total of over 80 distinct proteins. The best known and major group is the Dbl family, defined by a Dbl homology (DH) domain and a pleckstrin homology (PH) domain, C-terminal to the DH domain (Rossman, Der and Sondek, 2005; Schmidt and Hall, 2002). The DH domain is necessary for GEF activity and the PH domain seems to have a role in assistance of exchange reaction (García-Mata and Burridge, 2007) and can help to target the RhoGEFs to their appropriate intracellular localization, however the precise role of this domain remains unclear (Etienne-Manneville and Hall, 2002; Schmidt and Hall, 2002). All the 23 RhoGEFs identified in *Drosophila* belong to the Dbl family. The DOCK (dedicator of cytokinesis) family has been defined more recently and is characterized by a conserved catalytic domain, DOCK homology region 2 (DHR2) and a phospholipid-binding domain (DHR1) that locates them to membranes (Côté *et al.*, 2005; Meller, Merlot and Guda, 2005). DOCK proteins are specific for Rac and Cdc42 (Côté and Vuori, 2007).

Interestingly, there are about four times more RhoGEFs than their target RhoGTPases. This suggests that a specific RhoGTPase could be activated by multiple RhoGEFs. This redundancy could be explained by the tissue-specific distribution of the RhoGEFs, despite the apparent broad expression of most RhoGEFs (García-Mata and Burridge, 2007; Goicoechea *et al.*, 2014). RhoGEFs present a huge variety of domain structures in addition to the core domains described above. These different domain structures could also contribute to the specific regulation of different signaling pathways by RhoGTPases (Goicoechea *et al.*, 2014). RhoGEFs can be regulated in a complex manner that is not still completely understood but can include protein-protein or

protein-lipid interaction, binding of second messengers and postranslational modifications. It is thought that these interactions can lead to three major changes in GEFs: translocation to specific compartment of the cell, release from an autoinhibitory state or induction of allosteric changes in the catalytic domain (Bos, Rehmann and Wittinghofer, 2007).

1.4.1 *Drosophila* Rho guanine nucleotide exchange factor 10

We have previously identified a *Drosophila* gene, *darhgef10*, which is strongly expressed in the developing heart between embryonic stages 13-17 (Mantas Dias, 2012). The *darhgef10* gene encodes a Drosophila Rho guanine nucleotide exchange factor (RhoGEF) homologous to a protein known as ARHGEF10 or RhoGEF10 in humans (Mantas Dias, 2012; Verhoeven *et al.*, 2003). Interestingly, deletion of *darhgef10* in *Drosophila* leads to subtle, yet prevalent embryonic heart abnormalities, consisting of misaligned cardioblasts in both the aorta and heart regions. Surprisingly, *darhgef10* mutant flies are viable, suggesting that the presence of the cardiac defects is compatible with unchallenged life under laboratory-growth conditions.

The human Dbl family member ARHGEF10 is a specific activator of RhoA (Aoki *et al.*, 2009; Chaya *et al.*, 2011) and was first identified as the product of a gene associated with slowed nerve conduction velocities of peripheral nerves (Verhoeven *et al.*, 2003). ARHGEF10 has a DH domain and a very divergent PH-like domain. Thus, it was considered to be a member of a Rho-specific GEF family with unusual protein architecture (Mohl *et al.*, 2006). The mouse ARHGEF10 homolog, GEF10, was found to be broadly expressed with highest levels in the heart and skeletal muscle (Verhoeven *et al.*, 2003). This expression pattern is consistent with the strong enrichment we find for *darhgef10* expression in the developing *Drosophila* dorsal vessel (Mantas Dias, 2012). In *Drosophila*, dArhgef10 has an insect specific N-terminal domain, which is encode by isoform C (Figure 7).

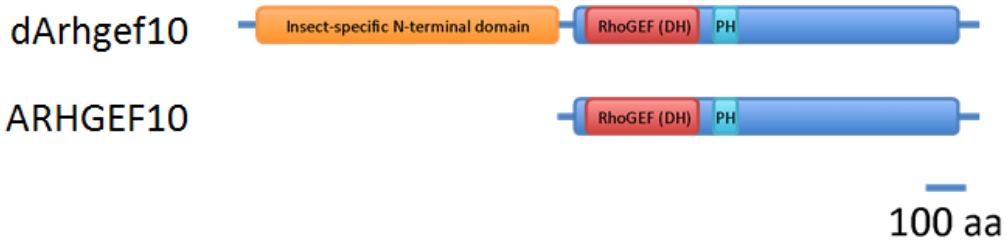

Figure 7 - Schematic structure of the Dbl member family ARHGEF10 and dArhgef10. DH represents the Dbl homology domain and PH, the pleckstrin homology-like domain. Although this RhoGEF possess a PH-like domain (blue region) it has a very divergent architecture when compared to other RhoGEF PH domains (Aoki *et al.*, 2009).

1.4.1.1 ARHGEF10 in cardiovascular and neurodegenerative disorders

We identified *darhgef10* as being a gene required for proper heart development in *Drosophila* (Mantas Dias, 2012). Interestingly, different studies have found a link between human *ARHGEF10* and atherotrombotic stroke or peripheral neuropathies (Matsushita *et al.*, 2010; Verhoeven *et al.*, 2003; Yin *et al.*, 2011).

In humans, a SNP in *ARHGEF10* was found to be strongly associated with atherothrombotic stroke. This single point mutation may cause increased levels of *ARHGEF10* transcript due to a higher affinity for the sp1 transcription factor, enhancing the RhoA-Rho kinase activity that contributes to the development of atherothrombotic stroke (Matsushita *et al.*, 2010). Indeed, the effector RhoA-Rho-kinase had already been implicated in the process of atherosclerotic cerebral infarction (Shimokawa and Takeshita, 2005).

Another mutation in *ARHGEF10*, which leads to an amino acid substitution of Threonine to Isoleucine (T332I), was identified in patients with slowed nerve conduction velocity, which was associated with thin myelination of peripheral nerves (Verhoeven *et al.*, 2003). This was the first time that *ARHGEF10* was identified as been implicated in peripheral-nerve conduction, suggesting a possible role for *ARHGEF10*

during the development of the peripheral nervous system in vertebrates. Cell culture experiments then suggested that the T332I change could confer constitutive GEF activity, because it maps within a large N-terminal domain that negatively affects *ARHGEF10* activity. Ectopic ARHGEF10 expression induces cell contraction in rat schwann cells, mediated by Rho-ROCK activity signaling, impairing schwann cell processes and consequently proper myelination (Chaya *et al.*, 2011).

More recently, a 10-bp deletion in the canine *ARHGEF10* was associated with a severe polyneuropathy in leonberger dogs. This pathology has many clinical similarities with Charcot-Marie-Tooth (CMT) disease in humans, a genetically heterogeneous group of peripheral neuropathies sharing the same clinical phenotype (Ekenstedt *et al.*, 2014;Pareyson, 1999). Once again, a possible role for *ARHGEF10* in controlling the development and/or maintenance of peripheral nerves was suggested.

1.4.2 *darhgef10* mutants

We have previously generated two *darhgef10* deletion mutations (deficiencies) by the FLP-FRT method (Mantas Dias, 2012; Parks *et al.*, 2004): a small and a large (big) deletion, hereafter termed *darhgef10[Df(1)ΔS]* and *darhgef10[Df(1)ΔB]*, respectively (Figure 8). The *Df(1)ΔS* covers at least three transcription start sites for the *darhgef10* gene and the non-coding RNA *CR44692*, while *Df(1)ΔB* covers the majority of the *darhgef10* coding region, including the DH and PH-like domain coding regions, and affects at least four other genes lying 5' of *darhgef10* (*CG8568*, *p-cup*, *CG5613* and *CG12994*). From this information alone we can predict that *Df(1)ΔB* is a dArhgef10 protein null allele.

Both *darhgef10* mutants are homozygous viable, suggesting that this gene is not essential for *Drosophila* development, however, both mutants showed a misaligned cardioblasts phenotype (Figure 9) (Mantas Dias, 2012).

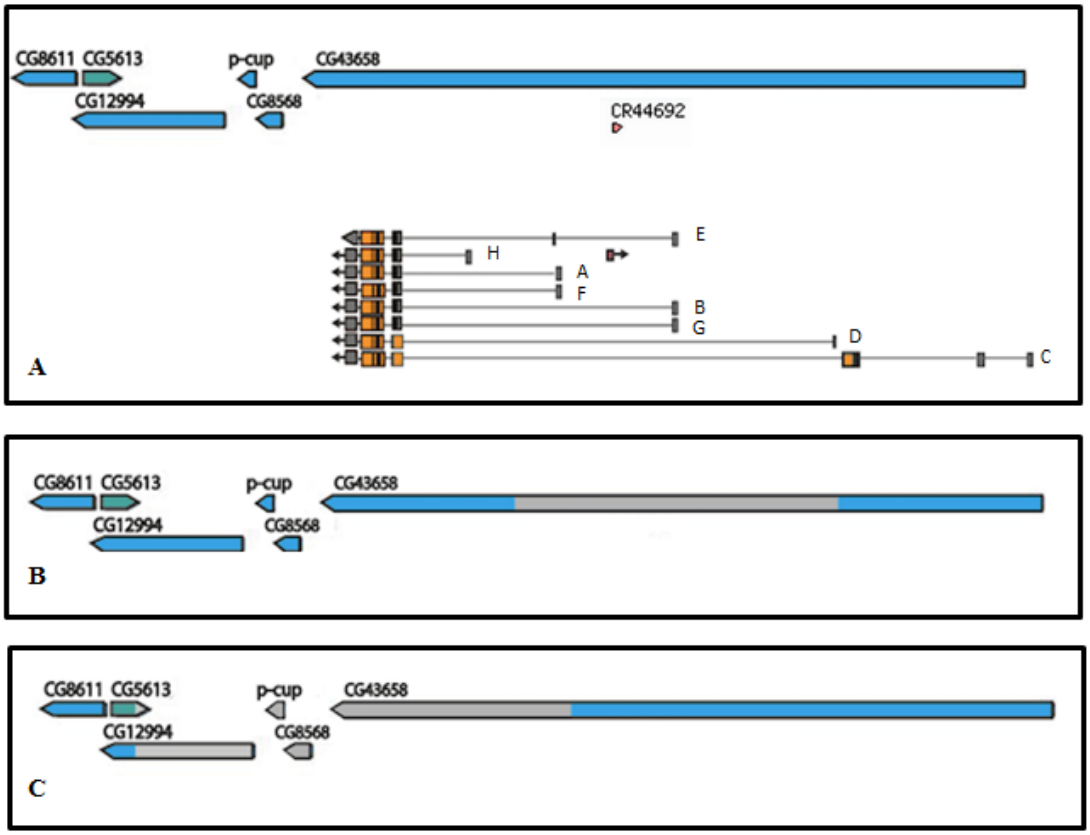

Figure 8 - Scheme of the *darhgef10* (aka *CG43658*) gene and the regions deleted in the *Df(1)ΔS* or *Df(1)ΔB* deficiency mutations (grey boxes). A - The *darhgef10* gene and 5 flanking genes on the X chromosome of *D. melanogaster*. All *darhgef10* transcripts are represented. B - The grey box depicts the region deleted in the *Df(1)ΔS* mutant. C - The grey box depicts the region deleted in the *Df(1)ΔB* mutant. Isoforms are indicated in A. Notice that four other genes are affected by *Df(1)ΔB*.

While *Df(1)ΔB* is clearly a protein null, *Df(1)ΔS* is not as some *darhgef10* isoforms are left intact by this *deficiency*. However, both *darhgef10 Df* mutations show the same phenotype of cardioblast missalignment. This is explained because the *Df(1)ΔS* removes the transcriptional promoter of two of the major isoforms of *darhgef10* (isoforms B and E) (Figure 8). Consequently, the total transcript levels in *Df(1)ΔS* are reduced by >80% in this background (annexes figure I; Heredia, Mantas Dias and Gontijo, unpublished results). *In situ hybridization* studies showed that no *darhgef10* transcript is detectable in the developing cardioblasts in *Df(1)ΔS* embryos, suggesting that the isoforms B & E are responsible for most, if not all, cardioblast

expression. Thus, even though *Df(1)ΔS* is not a protein null, it is a strong reduction of function and could likely be a null for many cell types, including the developing cardioblasts, explaining the phenotypic similarity between *Df(1)ΔS* and *Df(1)ΔB.*

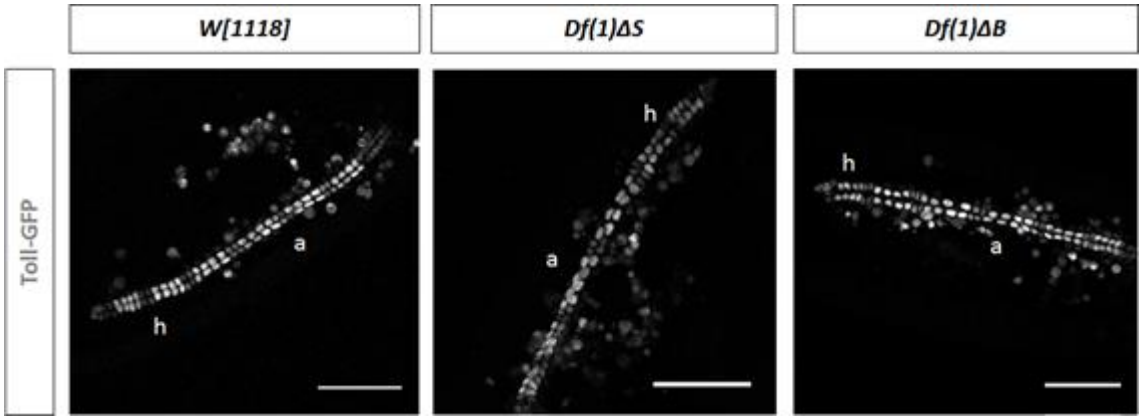

Figure 9 - Dorsal vessel visualized with a Toll-GFP reporter line showing the misaligned cardioblasts phenotype found in *darhgef10* mutants (a indicates the aorta region and h the heart region). Scale bars: 50µm. Adapted from (Mantas Dias, 2012).

1.5 Aims

Our aims were to phenotypically characterize the newly generated *darhgef10* mutants by surveying their development, viability, lifespan and behavior, and in parallel to investigate the cellular basis of their misaligned cardioblasts phenotype. Since human *ARHGEF10* is a susceptibility gene for cardiovascular diseases (Yin *et al.*, 2011; Matsushita *et al.*, 2010), we intend to explore *darhgef10* mutants as potential models to study the interaction between environmental challenges and a congenitally compromised circulatory system.

Chapter 2. Materials and Methods

2.1 Fly strains and husbandry

In this work, all fly stocks were maintained at 18ºC and raised in standard cornmeal-agar medium. When performing experiments, animals were grown at 25 ºC in appropriate humidity conditions at 75 % to achieve a controlled life cycle of about 10 days.

Virgin female collections and *Drosophila* stocks maintenance were performed as described by Ashburner (Ashburner and Roote, 2007).

All *Drosophila* stocks used in this study are described in Table 1. The stocks were obtained either from the Bloomington Drosophila stock center (http://flystocks.bio.indiana.edu/), from the Vienna Drosophila Resource Center (http://stockcenter.vdrc.at/control/main), from other laboratories as a gift or were generated in our laboratory, as depicted below.

Table 1 - Drosophila melanogaster stocks used in this work.

Name	Genotype	Stock	Source
W^{1118}	*w[1118]*	NA	Gift from Maria Dominguez
ΔS	*darhgef10[Df(1)ΔS]*	NA	Gift from Antonio Jacinto
ΔB	*darhgef10[Df(1)ΔB]*	NA	Gift from Antonio Jacinto
ey-gal4	*ey-Gal4/CyOactGFP*	NA	Gift from Maria Dominguez
Rho1 RNAi	*Rho1 RNAi (II)*	16042	VDRC
RNAi dArhgef10	*y[1] sc[*] v[1]; P{y[+t7.7] v[+t1.8]=TRiP.HMS00332}attP2*	32341	BDSC

Rho1 mutant	*w[*]; b[1] pr[1] cn[1] Rho1[1B] px[1] sp[1]/CyO*	9477	BDSC
Recombinant	*ey-Gal4>pTW::CG43658/CyOGal80*	NA	Generated in our lab
Oregon	*Oregon-R-C*	5	BDSC
FM7	*Ngr[l4]/FM7c*	5708	BDSC
Lifeact_ΔS	*darhgef10[Df(1)ΔS];;UAS-lifeactGFP,MefGal4/TM6b*	NA	Generated in our lab
Lifeact_ ΔB	*darhgef10[Df(1)ΔB];;UAS-lifeactGFP,Mef2Gal4/TM6b*	NA	Generated in our lab
Rock mutant	*Y[1] W[1118]Rok[2] P{ry[+t7.2]=neoFrt}19A/FM7c*	6666	BDSC
Rho1 mutant	*W[a] N[fa-g]; Rho1 [E3.10]/CyO*	3176	BDSC
Rok1 mutant	*W*Rok1/FM7i,P{actGFP}JMR3*	6665	BDSC
Rock RNAi-TRIP	*y[1] v[1]; P{y[+t7.7] v[+t1.8]=TRiP.JF03225}attP2*	28797	BDSC
Rho1 RNAi	*Rho1 RNAi-kk (II)*	109420	VDRC
Rock RNAi-kk	*DRHK RNAi-kk (II)*	104675	VDRC
Diaphanous RNAi	*y[1] v[1]; P{y[+t7.7] v[+t1.8]=TRiP.HM05027}attP2*	28541	BDSC
ΔS_iso	*darhgef10[Df(1)ΔS];iso;iso*	NA	Generated in our lab
ΔB_iso	*darhgef10[Df(1)ΔB];iso;iso*	NA	Generated in our lab
Lifeact	*;;UAS-lifeactGFP,MefGal4/TM6b*		Gift from Antonio Jacinto
Double balanced	*w; If/CyO;MKRS/Tm6b*	NA	Gift from Antonio Jacinto

2.2 Phenotypic characterization of *darhgef10* mutants

darhgef10 mutations cause subtle heart abnormalities that arise during embryonic development. To learn more about the possible effects of these abnormalities on other developmental and life history traits and/or to identify novel *darhgef10*-dependent phenotypes we characterized a series of parameters of *darhgef10* animals, including larval development and adult viability, fecundity, longevity and negative geotaxis behavior of adult flies.

2.2.1 Viability and fecundity assays

To study the fertility of *darhgef10* mutant flies, we performed fecundity and viability assays. The fecundity consists in the number of eggs that a single female laid per hour and viability is based on the number of eggs delivered by a single female per hour that hatch to larvae.

For these experiments, the adult flies were raised in optimal developmental conditions (with a controlled number of eggs per vial to avoid overcrowding, and controlled temperature at 25 ºC) in order to minimize any nutritional and/or environmental negative effect on their fecundity (such as a reduction on ovariole number). A day before (24 h) each fecundity/viability experiment, 5-10 virgin females and an equal number of males all aged between 3 to 7 days old were crossed. The flies were kept in laying pots for 6 h and apple plates were replaced every 2 h. After 6 h, the eggs laid during the day were transferred to a strip of paper impregnated in 1x PBS and counted. The strip of paper was transferred to a new vial and viability analysis was performed 24 h later by scoring the number of eggs that hatched. This procedure was repeated for 3 consecutive days and each fly that died or escaped was discounted in the egg/female ratio. The fraction of larvae that pupariated and then eclosed into adults were registered for each genotype as further indicators of viability. The fecundity and viability measurements between genotypes were compared using analysis of variance (ANOVA) followed by post-hoc Tukey's HSD (honest significant difference) test, using $\alpha = 0.05$.

2.2.2 Developmental time assay

In order to verify if *darhgef10* larvae had any major problem developing as larvae, we measured the time they took to pupariation. If *darhgef10* affected heart physiology, maybe the larvae had difficulties in any of the behaviors required to reassure the rapid growth necessary to achieve a typical timing of the onset of metamorphosis. We therefore performed pupariation assays following the development of synchronously growing larvae until reaching the pupal stage.

As in the fertility assay, flies were crossed 24 h before starting the assay and kept at 25 ºC in a laying pot. In each day of the assay, flies laid eggs during 9 h in a laying pot with an apple plate that was switched every 3 hours. 48 h AEL (after egg laying), the larvae were transferred to vials, usually 3 vials of 10 larvae each, to avoid overcrowding. This was repeated in 3 consecutive days. Two days following transfer of the larvae, we started scoring time of pupariation for each larvae by counting pupae at 10 am, 3 pm and 7 pm, until all larvae had pupariated. Statistical analyses was performed using the Wilcoxon rank sum test followed by bonferroni–holm method for *p*-value adjustment to multiple comparisons, using $\alpha = 0.05$.

2.2.3 Negative geotaxis behavior assay

In *Drosophila*, negative geotaxis is an innate behavior where flies preferentially move against the gravitational force when agitated. This can be observed by their tendency to climb up a tube after the tube with the flies is tapped on a table top. To perform this behavior the flies require an intact locomotor capacity. Not surprisingly, this behavior declines with the age of the animals and is affected by mutations in genes that affect locomotor activity**.** Our aim with this experiment was to use the negative geotaxis behavior assay as an indicator of the overall locomotor capacity of the *darhgef10* mutant lines as compared to their controls (*w[1118]* background). In other words, we wanted to see if the congenital heart defect in the mutant lines leads to a reduced locomotor behavior capacity of the flies (Nichols, Becnel and Pandey, 2012).

For this assay, newly emerged adult male flies were collected in a total of 5 sets of 10 male flies of each genotype, and kept at 25 ºC during the experiment. In order to follow the height climbed for each flies, we used a tube with a 2 cm, 4 cm and 6 cm mark. To perform the assay, the tubes were sharply tapped down three times, ensuring that each tap is hard enough to knock down all the flies to the bottom of the tube. The behavior of the flies was followed by a video camera during 10 s. After this time, the number of flies that passed 2 cm, 4 cm and 6 cm was registered. This procedure was repeated 10 times for each set of flies analyzed, with a 30 s interval between each assay to allow the flies to recover. The assay was performed with male flies aged 1, 20, 40 and 60 days after eclosion. Statistical analysis was performed using Fisher's test followed by Bonferroni Correction (α/n) for multiple comparisons, using α=0.05.

2.2.4 Longevity assays

In order to study the influence of *darhgef10* on total lifespan, we performed a longevity assay, following the flies from adult eclosion until death. Newly emerged adult flies, grown in optimal developmental conditions (with a controlled number of eggs per vial to avoid overcrowding, and controlled temperature at 25 ºC) were collected. The collection day was established as day 0. The vials were changed twice a week, allowing optimal growth conditions (food supply and media texture) in order to guarantee more robust data. Thereby, the possibility of the recorded deaths happening because of environmental conditions instead of the age factor in study is reduced. Data was analyzed statistically using the log rank test (http://bioinf.wehi.edu.au/software/russell/logrank/) followed by Bonferroni Correction (α/n) for multiple comparisons, using α=0.05.

2.3 Targeted genome editing using CRISPR-Cas 9

2.3.1 Guide RNA and repair cassette design

In order to access the localization of dArhgef10 protein, we used a CRISPR-Cas9 mediated homologous repair-based technique (Jinek *et al.*, 2012; Port *et al.*, 2014) to tag this protein with a green fluorescent protein (*sf*GFP) and OLLAS (E.coli OmpF Linker and mouse Langerin fusion Sequence) at its Amino (C)-terminus, separated by two flexible linker spacer sequences GSGSGS.

The guide RNA (Figure 10) was designed with http://tools.flycrispr.molbio.wisc.edu/targetFinder, synthetized by Sigma and cloned into pU6-BbsI-chiRNA.

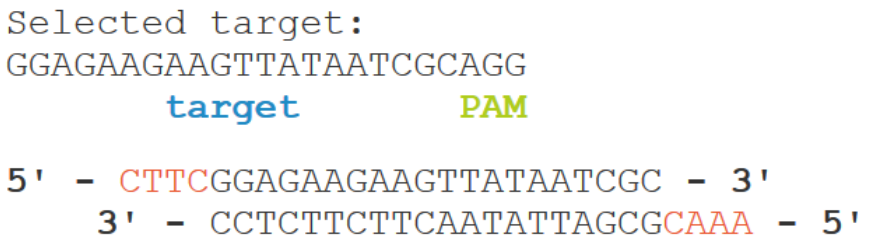

Figure 10- GuideRNA used in the CRISPR-Cas9 strategy with PAM sequence. Nucleotides represented in red are only used to clone into pU6-BbsI-chiRNA.

The repair cassette was synthesized *de novo* and cloned into a pUC57 plasmid by GeneScript and co-injected, by BestGene, with the gRNA into w^{1118}; *PBac{y[+mDint2]=vas-Cas9}VK00037/CyO,P{w[+mC]=Tb[1]}Cpr[CyO-V]* embryos, which expresses *Cas9* under control of *Vas* regulatory sequences. The following sequence corresponds to the repair cassette, where dark blue corresponds to the homology region after *darhgef1*0 end, dark red to the homology region up to *darhgef10* end, green to the *sf*GFP, blue to the spacers (GSGSGS), grey to the OLLAS epitope, brown to the restriction site for BglII and orange to the restriction site for AgeI:

GCCAGCCGCCGCGGTGGCCACTTTAAAGCGAAAACAGAAGCAGAACTCCAAGCAGCAGCAGCAACAGAACGCCGACG
GACCAAGGACAGTGATCACCCTGATGGGCGGACGCGGCTACTGGCGCCAGATGTGGTACAACGGGGCGGGTGGTTCG
CCCAGCCATAAGAACAGCAGCTCCGGCGGCGGCGGAGGCAGTGGCTCCGGATTCAGTGGCCAAACAATGCAGTCGGG
TAATCCCAGCTGCTCACCGCTGACGGCCAACTCCAATGACGCCCACATCGTTGTCTGGGAGAAGAAGTTAGGCTCCG
GTAGTGGTTCCAGATCTCGTAAGGGCGAGGAGTTGTTCACGGGAGTTGTGCCCATATTGGTTGAGCTGGATGGAGAT
GTGAATGGCCACAAGTTCAGTGTGCGGGGTGAGGGAGAAGGAGACGCAACAAACGGTAAGCTGACACTGAAGTTCAT
TTGTACTACGGGCAAGCTCCCGGTGCCATGGCCCACATTGGTCACCACCCTGACCTATGGCGTGCAATGCTTCGCCC
GATATCCAGATCATATGAAGCAGCATGATTTCTTTAAGTCGGCCATGCCCGAGGGTTACGTACAAGAGCGCACTATT
AGCTTTAAGGACGACGGTACGTATAAAACCAGGGCTGAGGTGAAGTTTGAGGGTGATACCCTGGTGAACCGCATTGA
ATTGAAGGGCATCGATTTTAAGGAGGACGGCAACATCCTGGGCCACAAGCTCGAATATAATTTTAATAGCCATAATG
TTTACATTACCGCGGACAAGCAGAAGAATGGAATTAAGGCTAATTTCAAGATCCGACATAATGTGGAGGACGGATCC
GTTCAGTTGGCCGATCACTACCAGCAAAACACCCCCATCGGAGATGGCCCCGTCCTGCTGCCCGATAACCACTACCT
GAGTACCCAGTCCGTCCTGTCGAAGGATCCTAATGAGAAGCGGGATCATATGGTGCTGCTGGAGTTTGTGACTGCCG
CCGGCATAACGCATGGAATGGACGAGCTGTATAAAGGCTCCGGTAGTGGTTCCTCCGGCTTCGCCAACGAGCTGGGC
CCCCGCCTGATGGGCAAGACCGGTTAATCGCAGGAGCTGGTGTGCTGCTGCACCCTTCAGCAGCATCCCCACCAGCA
CCATCCACCGCTAACCGAGCTGTGGCGCCGCGTGGGCGAGCAGCATCAGCAGCACCAGCAGCTGCAGCAGGCGCAGC
GTCGTGGCCGTGGACGGGTCCGGTTCCGGGGATCCTTTATTCAGCGGGATCGCAGTGCCGGCAGCGATGGAGGAAGC
GGTTACGGATCAGGCGGATTGTCAGGTGCTGGCGGATCGGGGGGCATGTTGGGTGCCAGTCTGAAGCGACTGACCAA
GCTAAAGCGCGGCGGCA

The adults originating from the injected embryos, hereafter refered to as founder flies, were separately crossed with *Ngr*^{l4}*/FM7c* flies. Since *darhgef10* is on the X chromosome, we followed two different strategies depending on whether the founder flies were male or female: 1) For female founders, either male or female F1 progeny were separately crossed again with *Ngr*^{l4}*/FM7c*; 2) For male founders, only the F1 female flies were crossed again with *Ngr*^{l4}*/FM7c*. After eclosion of the F2, we extracted genomic DNA (gDNA) from single F2 male flies and performed PCR to search for insertion of the repair cassette in the genome.

2.3.2 Screen for mutants

For gDNA extractions, we isolated a single male fly, which was macerated with a pestle homogenizer in 100 µl of DNA Extraction Buffer (1 M Tris-HCl, pH 8.2, 0.5 M EDTA, 5 M NaCl). When properly homogenized, we added 1 µl of Protease K 50 ng/µl (Roche) followed by 1h incubation at 37°C. To inactivate the protease, gDNA was incubated at 95 ºC for 5 min. gDNA was stored at -20ºC.

We used two sets of primers to look for mutants, designed and tested for specificity using Primer – BLAST (http://www.ncbi.nlm.nih.gov/tools/primer-blast/) and synthetized by Sigma (USA). Primers were designed to check for the presence of the repair cassette from the right and left side of the target region (Table 2 and Figure 11).

Table 2 - Primers used for gDNA PCR amplification in CRISPR-Cas9 screen.

Primer name	Primer sequence (5'→3')	Fragment size (bp)
Pair 1:		
CG43658_Guide1_check_R	CCAAGCCAGATGAGATGAGC	975
SuperfolderGFP_F	CAGCACCATATGATCCCGCT	
Pair 2:		
CG43658_Guide1_check_F	CCGCCGGTTTTTGAGCCTAA	1034
SuperfolderGFP_R	CCTATGGCGTGCAATGCTTC	
Pair 3:		
CG43658_Guide1_check_R	CCAAGCCAGATGAGATGAGC	587
SuperfolderGFP_RC_F	GAAGCATTGCACGCCATAGG	

Figure 11 - Scheme of primers recognition sites used for CRISPR-Cas9 screen.

PCRs were performed in a T100® Thermal Cycler (Bio-Rad) using a Supreme NZYTaq 2x Green Master Mix (NZYtech), with premixed dNTPs, polymerase, a source of Mg^{2+} and a dye.

Table 3 - Standard PCR reaction used in CRISPR-Cas9 screen

Reagent	Final concentration	Volume
Supreme NZYTaq 2x Green Master Mix	0.2 U/µl	5 µl
Primer forward	1µM	0.5 µl
Primer reverse	1µM	0.5 µl
***MiliQ* water**	-	3 µl
Genomic DNA	-	1 µl
		10 µl

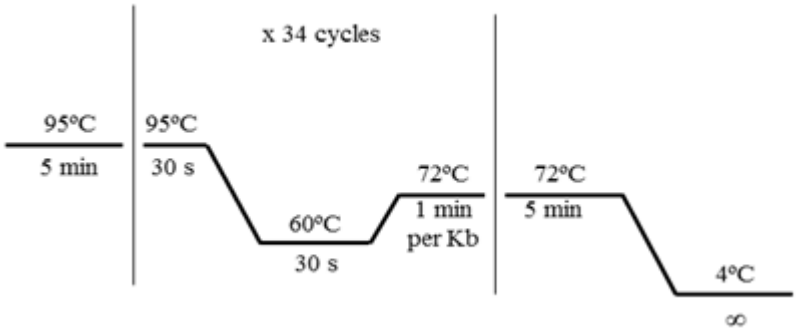

Figure 12 - PCR program used for all gDNA amplifications in CRISPR-Cas9 screen

PCR products were subject to electrophoresis in a 1.2% agarose (NZYTech) gel in TAE 1x buffer (G-Biosciences). In order to visualize DNA we added 2 µl of Green Safe Premium (NZYTech) per 50 ml of agarose gel and the NZYDNA Ladder III (NZYTech) was used as a molecular weight marker. Electrophoresis was performed at 100 V for ~30 min in a PowerPac 300® (Bio-Rad) system. PCR products were

visualized under UV transillumination in a Molecular Image Chemidoc™ XRS+ (BioRad).

2.4 Live imaging

2.4.1 Embryo collection

To collect embryos, an approximately equal number of male and female adult flies of each genotype were introduced in a laying pot attached to an apple plate, at least two days before the collection. The plates were switched daily and a small amount of yeast paste was spread to encourage females to deposit eggs.

In the day before the collection, apple plates were switched to new ones and laying pots were kept overnight (~16 h) at 25 ºC. In the next day, the excess of yeast paste was removed and embryos were collected from apple plates by rinsing with dH_2O. With the help of a brush, embryos were collected to a 70 μm nylon cell strainer and washed with dH_2O. In order to remove the chorion membrane, the cell strainer with embryos was immersed into 50% bleach for approximately 1 min, visualizing the process in a stereoscope. After this process, the bleach was removed by washing the embryos with dH_2O.

2.4.2 Mounting and imaging

After dechorionation, embryos in the developmental stages of interest were selected under a fluorescence stereomicroscope (SteREO Discovery V8), and gently aligned on a glass bottom petri dish (MatTEK corporation) with previously added embryo-glue (1 ml heptane + 3 cm double-sided tape) to stick the embryos. Embryos were immersed in Halocarbon Oil 27 (Sigma) and imaged immediately.

Imaging was performed in the confocal microscope Andor Spinning disk and images were analyzed using Fiji software (Schindelin *et al.*, 2012).

2.5 SL2 cells

2.5.1 Cell culture

For all cell culture dependent assays we used Schneider's Drosophila Line 2 [D. Mel. (2), SL2] cells (hereafter named as S2 cells), which is a cell line derived from a primary culture of late embryonic developmental stage (20-24 h) of *Drosophila melanogaster*. These cells grow between a state of semi-adherent monolayer and suspension and are routinely cultured in Schneider's *Drosophila* medium (Biowest) supplemented with 10% heat inactivated Fetal Bovine Serum (GIBCO Life Technologies) and 1% Penincilin-Streptomycin (Sigma), in a tissue culture T25-flask at 25 ºC. At least once a week cells were split in 1:10 dilution to a new T-flask.

For cell counting, 20 µl of the culture was diluted in 80 µl of Schneider's medium. Next, 20 µl of the diluted culture was added to equal volume of trypan blue reagent. Cells were counted in a hemocytometer (Neubauer chamber), having in consideration the 1:10 dilution. Trypan blue enables us to test cell viability, as live cells with intact cell membranes exclude the blue dye.

2.5.2 Transfection

Transfections were performed with the FuGENE® HD Transfection Reagent (Promega) according to manufacturer's protocol. FuGENE® is a nonliposomal reagent that enables the transfection of DNA into a wide variety of cell lines.

One day before transfection, $4x10^5$ cells were plated in a 24-well plate and grown in Schneider's medium supplemented only with 10 % FBS, as the antibiotic may adversely affect the process. For transfection, plasmid DNA was mixed with FuGENE® HD Transfection Reagent in a 3:1 FuGENE® HD Transfection Reagent:DNA ratio, and incubated for 15 min. After incubation, the mixture was added to the cells, mixing gently. Cells were incubated at 25ºC and assayed 48 h later.

2.6 Immunofluorescence assays

2.6.1 Sample preparation

2.6.1.1 Embryo fixation

The collection of embryos was performed as described in 2.4.1. Embryos were then fixed in a solution of 1:1 4% paraformaldehyde (Sigma) in 1x PBS: heptane (Sigma) in a glass scintillation vial for 40 min at RT with shaking. With a pasteur pipette, the fixed embryos were transferred from the vial to a new cell strainer, gently placed in a double sided tape and emerged in 1x PBS. Vitelline membranes were removed under a stereoscope with a thin glass needle. Lastly, embryos were transferred into a microcentrifuge tube and rinsed immediately with PBST (PBS with 0.3% Triton-X (Sigma)).

2.6.1.2 Larva dissection and fixation

In order to collect larvae, female and male adult flies were crossed and maintained in a vial at 25 ºC in standard fly food with a controlled number of animals to avoid overcrowding. We used wandering third instar larvae that appear after ~5 d.

Larvae were collected and placed in a dissecting dish filled with cold 1x PBS, and the desired tissues (brain, imaginal disc and/or salivary glands) were gently dissected preferably still attached to the carcasses to minimize loss of material and easy handling. Dissected material was immediately fixed in a fixative solution (4% formaldehyde in 1x PBS) for 30 min, at RT. After fixation, structures were rinsed with PBST to permeabilize cell membranes.

2.6.1.3 S2 cells

In order to harvest the cells, cell cultures were transferred to a microcentrifuge tube and centrifuged. The pellet was washed in 1x PBS to remove cell debris. Fixation was performed with 4 % paraformaldehyde (PFA) in 1x PBS for 15 min. The PFA solution was then removed and cells were washed with 1x PBS. Cells were permeabilized with

PBST and immediately before blocking, cells were washed with PBSTw (PBS + 0.1% Tween-20).

2.6.2 Antibody Staining

After permeabilization, blocking was performed by incubation with PBST supplemented with 1% BSA (m/v) for at least 1 h at RT or overnight at 4 ºC to avoid nonspecific binding of the antibodies. Embryos and larval tissues were incubated with primary antibody diluted in blocking solution overnight at 4 ºC followed by PBST washes. Next, the secondary antibody diluted in blocking solution was added and incubation was performed during 2 h at RT, protecting the samples from light exposure from this step on. The samples were washed with PBST, the nuclei were counterstained with 1:1000 DAPI (Sigma) solution for 5 min, washed with PBST, and finally washed with 1x PBS. The same protocol was followed for S2 cell immunofluorescence analyses, with the exception that PBSTw was used instead of PBST.

Antibodies used in the assays are described in table 4.

2.6.3 Mounting and Imaging

All samples were mounted in DABCO mounting medium (16 mL glycerol, 4 mL 1x PBS and 0.4 g DABCO) in microscope slides, and stored at 4 ºC protected from light. Imaging was performed in a Zeiss LSM 710 Confocal Microscope and images were analyzed using FIJI software (Schindelin *et al.*, 2012).

Table 4 - Antibodies and other dyes used in imunofluorescence assays.

Primary antibodies			
Protein	**Host**	**Concentration**	**Origin**
GFP	Rabbit	1:200	Life technologies, A11122
Talin A22A Talin E16B	Mouse	1:20	DSHB
Rho1	Mouse	1:50	DSHB, p1D9
Integrin β-PS1	Mouse	1:20	Gift from Antonio Jacinto
dArhgef10 (PAB#3)	Rat	1:50	Synthesized by metabion
Secondary Antibodies			
Name	**Host**	**Concentration**	**Origin**
Alexa fluor 488, anti-rabbit	Goat	1:250	Invitrogen
FarRed (Cy5), anti-mouse	Goat	1:250	Jackson Immuno Research
Alexa fluor 56, anti-rat	Goat	1:250	Gift from Antonio Jacinto
Alexa fluor 594, anti-mouse	Goat	1:250	Invitrogen
Phalloidin			
Name		**Concentration**	**Origin**
Phalloidin Alexa Fluor 568		1:200	Invitrogen
Phalloidin Alexa Fluor 488		1:200	Invitrogen

2.7 Immunoblotting

2.7.1 Sample preparation

S2 cells were resuspended and collected from the 24-well plates 48-h after transfection. In order to isolate the cells, all culture medium was centrifuged for 5 min at 800 g and the pellet was washed with ice-cold 1x PBS followed by centrifugation. To lyse the cells and extract the proteins, 2x Laemmli Sample Buffer (Biorad) with β-mercaptoethanol (Sigma) was added directly to the pellet. To ensure rupture of cell membranes, cells were smashed with a pellet pestle and lysates were boiled at 95ºC for 5 min to guarantee protein denaturation. After centrifugation at 12 000 g for 10 min at 4 ºC, the supernatants were used in a Western blot assay.

2.7.2 Western blot

Proteins samples were separated by sodium dodecyl sulfate polyacrylamide gel electrophoresis (SDS-PAGE). Protein samples were loaded into a 7.5% acrylamide gel and electrophoresed in a running buffer containing 25 mM Tris base, 192 mM glycine and 0.1% (w/v) SDS at 120 V for approximately 1 h, using the BioRad Mini-PROTEAN system.

After gel-separation, the proteins were transferred to a PROTRAN BA 85 Nitrocellulose membrane 0.45 µm (Whatman) by electrophoretic transfer (transfer buffer: 150 mM glycine, 20 mM Tris, 0.037% SDS, 20% (v/v) ethanol 96%, performed at 10 V for 1 h using a Mini Blot Module.

In order to prevent non-specific antibody binding, membranes were blocked in PBSTw supplemented with 5% (w/v) non-fat dry milk (Nestlé) for 30 min at RT with constant agitation. All proteins in the membrane were visualized with a Ponceau S (Merck) solution. Incubation with primary antibody, diluted in PBSTw supplemented with 1% (w/v) non-fat dry milk was done overnight at 4 ºC, under stirring. After

incubation, membranes were washed four times for 5 min each with PBSTw. Secondary antibody conjugated with a horseradish peroxidase (HRP) reporter was diluted in PBSTw and incubated for 1 h at RT, followed by four 5-min washes in PBSTw. Antibodies used in the assay are described in table 5.

To detect proteins of interest, the membrane was incubated in a 1:1 luminol:peroxide solution (Amersham ECL Prime Western Blotting Detection Reagent, GE Healthcare), for 5 min, in a process called enhanced chemiluminescence. Visualization of protein bands was performed in a ChemiDoc XRS+ system and exposure times varied depending on the target proteins.

Table 5 - Antibodies used in Western blot assays.

Primary antibodies			
Protein	**Host**	**Concentration**	**Origin**
dArhgef10 (PAB#1)	Rat	1:200	Synthesized by metabion
dArhgef10 (PAB#2)	Rat	1:200	
dArhgef10 (PAB#3)	Rat	1:200	
dArhgef10 (PAB#4)	Rat	1:200	
alfa tubulin	Mouse	1:1000	DSHB
Secondary Antibodies conjugated with HRP			
Name	**Host**	**Concentration**	**Origin**
Horseradish Peroxidase (HRP) conjugate	Goat	1:5000	Life technologies
Horseradish Peroxidase (HRP) conjugate	Rabbit	1:5000	SouthernBiotech

2.8 *ey>* screen for dArhgef10 effectors

To identify possible dArhgef10 effectors we performed a small screen. Our aim was to identify genes that encode proteins that could alter *darhgef10* activity. To ease this screen we expressed *darhgef10* under the control of the *eyeless* enhancer *ey-Gal4* (Figure 13) . This strategy uses the *Gal4/UAS* system to overexpress *darhgef10* in the eye disc primordia of embryos and in the eye imaginal discs of third instar larvae. *ey-Gal4>pTW::darhgef10* (*ey>darhgef10*) flies show deformed eyes, which are easily scored (Figure 14). Theoretically, this would give us a non-lethal combination, as the eye is not essential for *Drosophila* viability.

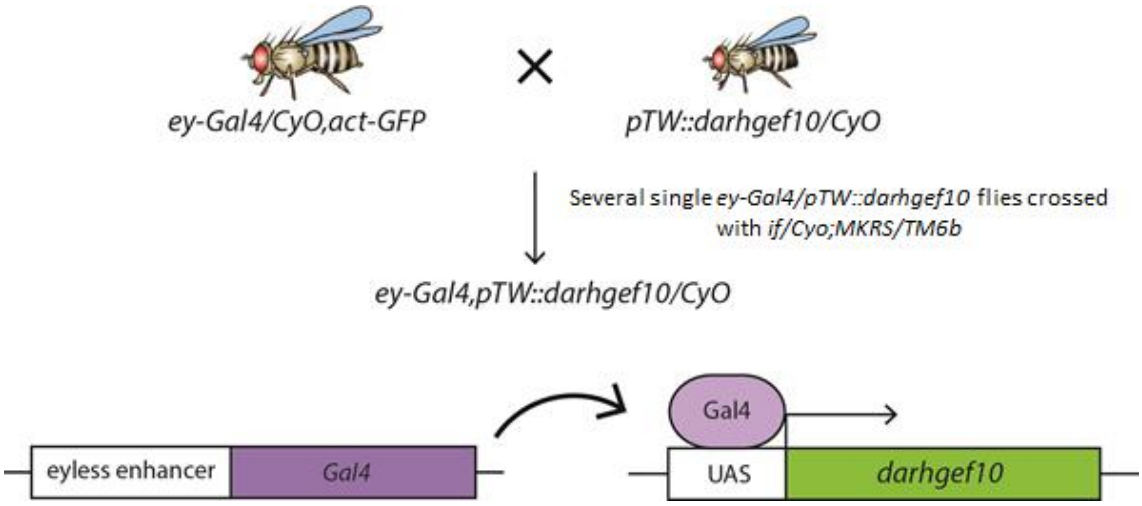

Figure 13 - Scheme used to create a recombinant construct line *ey-Gal4,pTW::darhgef10/CyO*.

In order to facilitate the screen we generated a recombinant line between *ey-Gal4* and *pTW::darhgef10.* Although we were able to obtain mix gender recombinant flies of the genotype *ey-Gal4>pTW::darhgef10/CyO*, the males were sterile so we had to keep this line balanced with *CyOGal80*, generating the stock *ey-Gal4>pTW::darhgef10/CyOGal80*. The yeast Gal80 protein binds to Gal4, inhibiting its transcriptional activation activity (Figure 15) (Pilauri *et al.*, 2005). This tool enables us to maintain a healthy stock and restrict the *ey>darhgef10* activity to single crosses where we remove the *CyOGal80* chromosome.

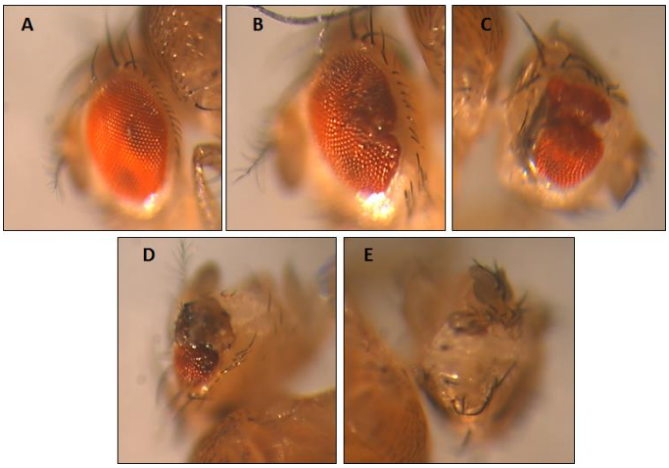

Figure 14 - Classification attributed to eye deformation in order to screen possible *darhgef10* effectors. A – score 1; B – score 2; C – score 3; D – score 4; E – score 5. Score equal to 1 correspond to a normal eye without deformation and the highest score correspond to the most severely deformed eye.

Since *darhgef10* expression with *ey-Gal4* driver leads to a phenotype of eye deformation, we used a set of mutants and RNAi lines against the genes *Rock*, *Rho1* and *diaphanous* to cross with the recombinant flies. Afterwards, the eye deformation observed in the flies with the genotype of interest was scored (as in Figure 14). Statistical analyses were performed using analysis of variance (ANOVA) test followed by post-hoc Tukey's HSD (honest significant difference) test.

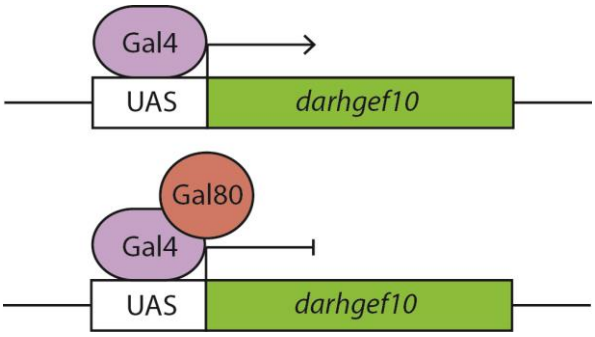

Figure 15 - Schematic representation of Gal4 dependent UAS expression repressed by Gal80. Image adapted from (Wu and Luo, 2006).

Chapter 3. Results and discussion

3.1 Phenotypic characterization of *darhgef10* mutants

In order to characterize phenotypically the *darhgef10* mutants, we performed several assays that enabled a fairly complete analysis. We studied the capacity of larvae to reach the pupal stage, evaluated the number and viability of the eggs laid by the *darhgef10* mutants females, analyzed the behavior and capacity of flies to ensure an anti-gravitational response and followed the lifespan of *darhgef10* mutants.

3.1.1 Developmental time assay

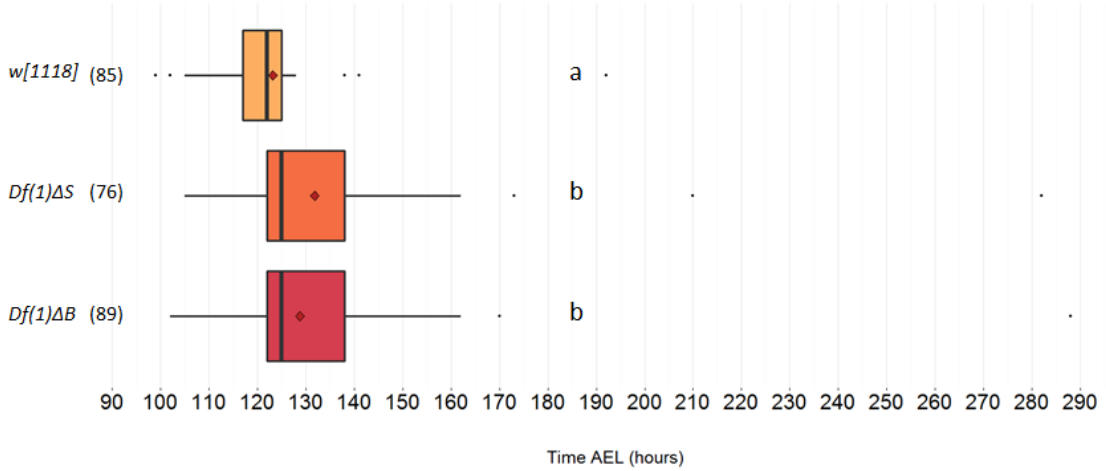

Figure 16 – Boxplots representing the pupariation time of (N) larvae. The assay compared the pupariation time of *darhgef10* mutant flies with the control *w[1118]*. Groups sharing the same letters are not statistically significant different at $\alpha = 0.017$, according to the Bonferroni-Holm correction for multiple comparison. Dot blots are outliers, dark bars correspond to the medians and red dots to the averages. Box limits indicate the lower and upper quartile and whiskers correspond to the maximum and minimum values, excluding the outliers.

First, to perform the phenotypic characterization, we tested if the time that *darhgef10* mutants took to reach the pupal stage is different relatively to the control *w[1118]* through a developmental time assay (Figure 16). In this assay we observed that both mutants, *Df(1)ΔS* and *Df(1)ΔB*, have a very small, yet statistically significant, 3 h delay in the onset of metamorphosis (*w[1118]* median = 122 h AEL, Df(1)*ΔS* and

Df(1)*ΔB* median = 125 h AEL; p<0.017). As the delay is found in both independent mutant lines, we are tempted to conclude that *darhgef10* is required to ensure normal developmental timing. However, since the delay is very small, it is hard to discuss the physiological relevance of this finding and to study its tissue and cellular origin further. Moreover, even though all lines are in a *w[1118]* background, we hope to repeat this experiment using isogenic lines and *Df(1)ΔB*/*Df(1)ΔS* transheterozygotes to exclude possible background effects and to gain confidence in these results.

3.1.2 Fecundity and viability assays

To investigate if the capacity to lay eggs is compromised in *darhgef10* mutants we did a fecundity assay, counting the number of eggs laid by a single female per hour (Figure 17). This analysis showed that none of the mutants have a significantly reduced number of eggs laid per hour relatively to the *w[1118]* control.

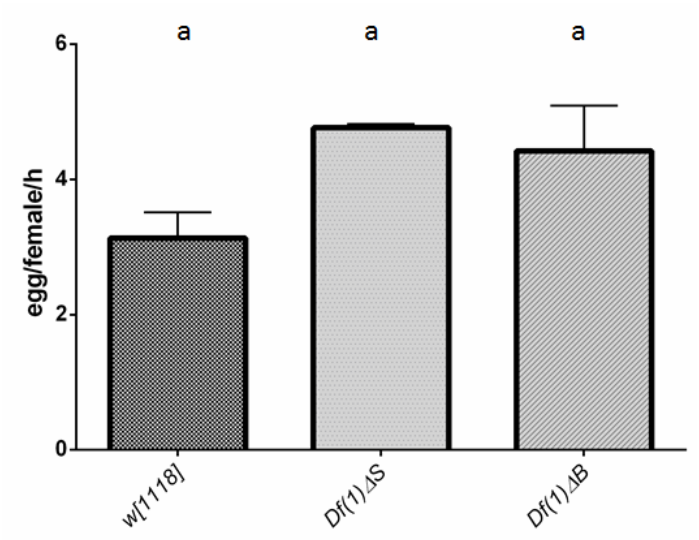

Figure 17 – Fecundity assay. Bar-graph describing the average number of eggs laid per hour by control (*w[1118]*) and *darhgef10* mutants females. Groups sharing the same letters are not statistically significantly different at α = 0.05, according to the Tuckey's HSD post-hoc test. N=3 for all experiments. Error bars represent the standard deviation of the mean (SD).

Despite the number of laid eggs not being reduced in the mutant lines, we did not know how many of these eggs were in fact able to hatch to larvae. We thus investigated what percentage of laid eggs originated adult flies, following each stage of development and registering the changes in viability between major life history transition events (egg to larva, larva to pupa and pupa to adult transitions; Figure 18).

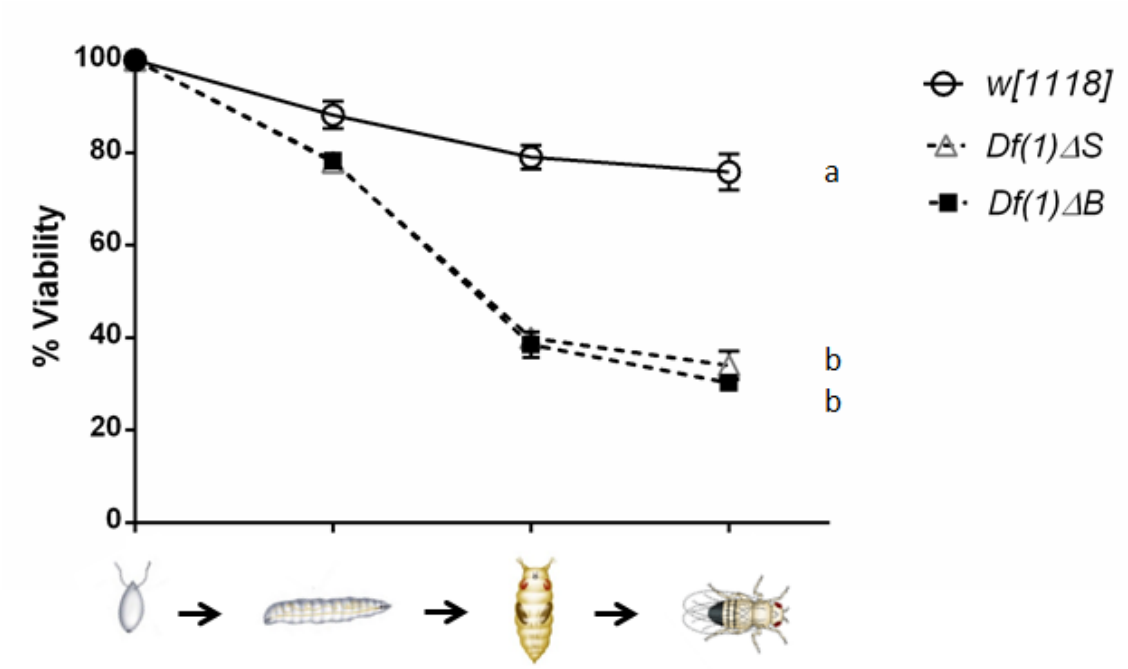

Figure 18 – Viability assay. Lines represent the percentages of viability through consecutive developmental stages. Total viability corresponds to the percentage of eggs that were able to reach the adult stage. All flies analyzed are isogenic. Groups sharing the same letters are not statistically significantly different at $\alpha = 0.05$, according to analysis of variance (ANOVA) for multi comparisons. N=9 for *w[1118]* and N=6 for both *darhgef10* deletions. Error bars represent the SD. Drawings were adapted from http://highered.mheducation.com/sites/dl/free/007352526x/873551/Reference D.pdf

Interestingly, we found a statistically significant ($p < 0.05$) reduction in the viability of either *Df(1)ΔS* or *Df(1)ΔB* when compared with *w[1118]* controls. Of all laid eggs, less than 40% *Df(1)ΔS* or *Df(1)ΔB* eggs originated adult flies. This corresponds to approximately half of the adult flies originated in the control line (~80%). A similar reduction in viability was found in *Df(1)ΔS/Df(1)ΔB* transheterozygote flies (Figure 19), suggesting that this effect is indeed linked to the *darhgef10* locus.

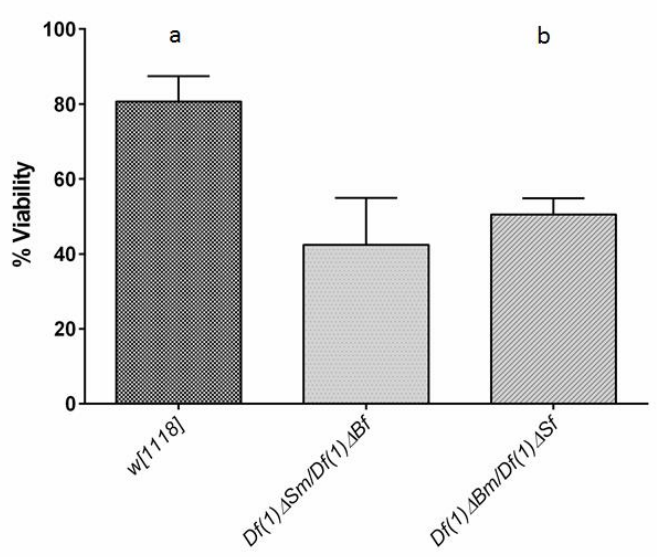

Figure 19 – Bar graph describing the percentage of eggs that reach the adult stage, laid by *w[1118]* females (control), *Df(1)ΔB* females mated with *Df(1)ΔS* males and *Df(1)ΔS* females when mated with *Df(1)ΔB* males, respectively. Groups with different letters are statistically significantly different at $\alpha = 0.05$, according to the Student's t-distribution. Statistical analysis was not performed to *Df(1)ΔSm/Df(1)ΔBf* due to insufficient set of sample elements. N=3 for all experiments except for *Df(1)ΔB* females mated with *Df(1)ΔS* males, where N=2. Error bars represent SD.

The analysis of the curves presented in Figure 18 indicate that even though the viability decreased in all phases, the major effect seems to occur during the larval phase. However, we do not know exactly in which particular larval stage the decrease in viability occurs as we only analyzed the number of eggs hatched, corresponding to the number of L1 larvae, and the number of pupae. The marked decrease in viability could happen at any time during the larval stage. As we did not observe any overt loss of viability in the L3 larvae selected for the developmental time assays described above in Figure 16, it is likely that the viability loss must occur either in the L1 or L2 stages.

Additionally, our analysis showed that the reduced percentage of adults obtained by a particular number of eggs cannot be exclusively explained by a problem during egg fertilization, since, approximately 80% of the eggs originated L1 larvae in all genotypes.

Next, in order to verify whether the observed reduced viability in *darhgef10* mutants, could be attributed to a maternal or paternal effect, we performed viability assays using *darhgef10* female flies crossed with males wild-type *Oregon* males and vice-versa (Figure 20).

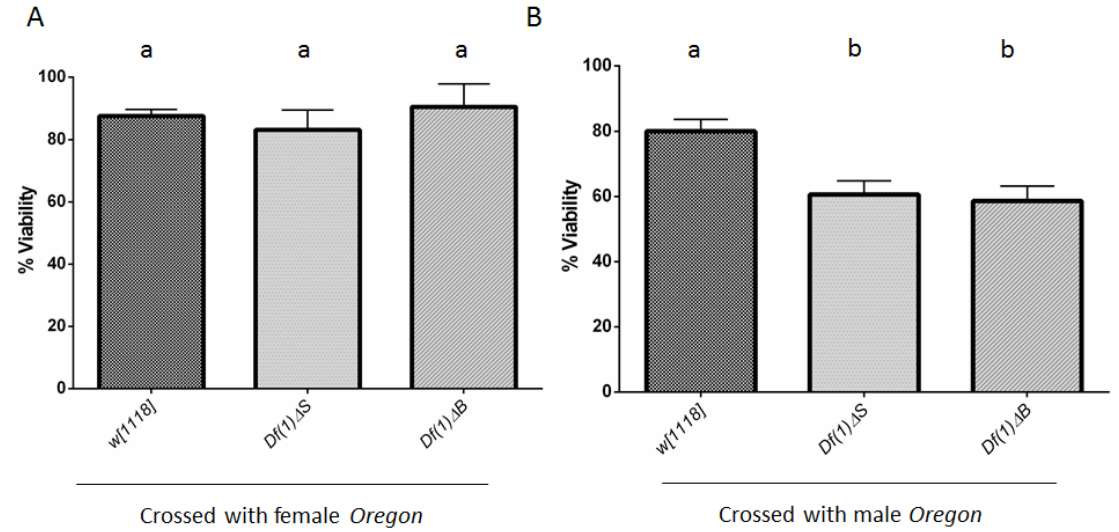

Figure 20 - Bar-graph describing the percentage of laid eggs that were able to reach the adult stage. A - Viability analysis using *Oregon* females crossed with *darhgef10* mutant males and with *w[1118]* males (control). B - Viability analysis using *darhgef10* mutant and *w[1118]* (control) females crossed with *Oregon* males. Groups sharing the same letters are not statistically significantly different at $\alpha = 0.05$, according to the Tuckey's HSD post-hoc test. N=3 for all experiments. Error bars represent the SD.

When we analyzed *Oregon* female flies crossed with *darhgef10* males we did not observe reduced viability when compared to the control *w[1118]* (Figure 20). This suggests that *darhgef10* males are perfectly capable of executing the complex behaviors related with copulation and fertilization. In contrast, when we analyzed *darhgef10* female flies crossed with *Oregon* males, we observed a statistically significant ($p < 0.05$) reduction of viability in both mutants. Of all laid eggs by the control females, approximately 80% originated adult flies, while only approximately 60% of the eggs laid by the mutant females originated adults, with an equivalent percentage of males and females. These results suggest that approximately half of the reduction in viability

observed in both *darhgef10* lines could be explained by a maternal effect. The other half of the reduction in viability must have a zygotic effect.

If the zygotic effect is indeed due to the loss of *darhgef10*, the effect should also be observed in transheterozygous *Df(1)ΔB/Df(1)ΔS* mutant flies. In contrast, if the effect is due to background mutations, it could disappear in these independent lines. We therefore crossed males *Df(1)ΔB* with females *Df(1)ΔS* and vice-versa (Figure 19). Transheterozygous mutants exhibit a accentuated reduction in viability, more than 30%, when compared to the control *w[1118]*. This viability reduction enable us to conclude that the zygotic effect could explain the additionally viability reduction in *darhgef10* mutants, that could not be explained by maternal effect.

3.1.3 Longevity assays

darhgef10 mutants have a congenital heart defect with misaligned cardioblasts in both aorta and heart region. Our viability experiments determined that a homozygous *darhgef10* mutation reduces the viability of flies by half (Figure 18). Next, we wondered whether the surviving adults had a normal lifespan. To answer this question, we performed longevity assays, following the *darhgef10* mutant flies from adult eclosion until death (Figure 21).

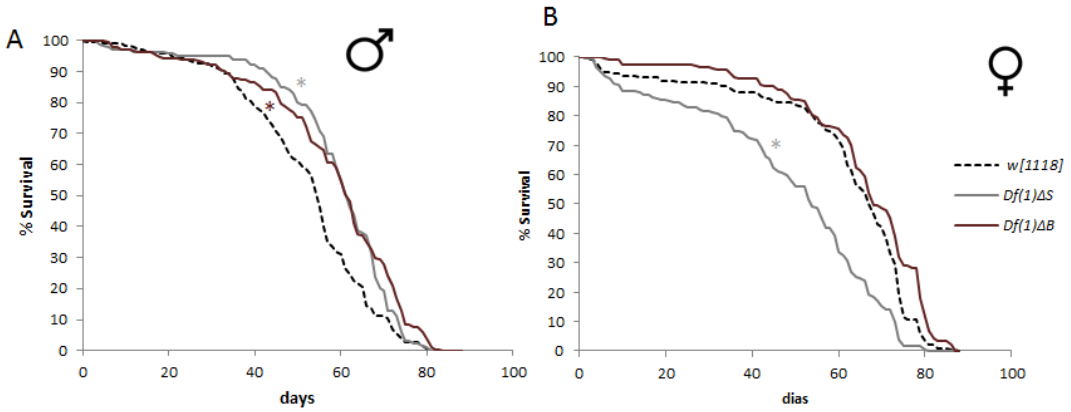

Figure 21 – Longevity of *darhgef10* mutants (*Df(1)ΔS* and *Df(1)ΔB*) and *w[1118]* control flies: A - males; B - females. Curves with asterisks are statistically significantly different from the others at α = 0.017, according to the log rank test (http://bioinf.wehi.edu.au/software/russell/logrank/). $N_{Df(1)\Delta S}$ = 179 (male), 183 (female); $N_{Df(1)\Delta B}$ = 203 (male), 181 (female); $N_{w[1118]}$ = 203 (male), 191 (female).

Surprisingly, we found that both *Df(1)ΔS* and *Df(1)ΔB* mutant males have a statistically significant increased lifespan when compared with *w[1118]* males. The same was not true for female flies. While *Df(1)ΔB* female lifespan was similar to *w[1118]* females, there was a statistically significant reduction in the lifespan of *Df(1)ΔS* females (Figure 21). These results were somewhat surprising. In order to gather independent evidence that *darhgef10* mutation could prolong the lifespan of males, we knocked-down *darhgef10* ubiquitously using the *armadillo-Gal4* (*arm>*) driver and an RNAi cassette against *darhgef10* (*UAS-darhgef10-IR*). Flies carrying *arm>* or the *UAS-darhgef10-IR* transgenes alone were used as controls (Figure 22).

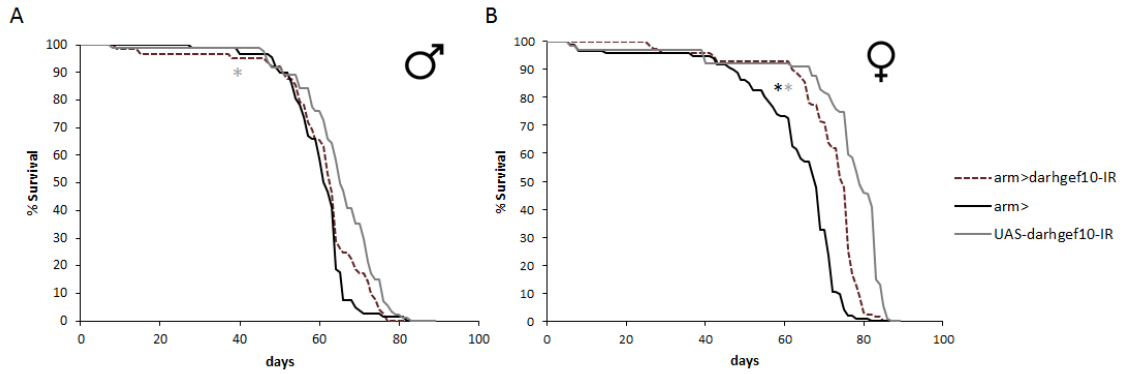

Figure 22 - Longevity of flies expressing constitutive RNAi against *darhgef10* (*arm>darhgef10-IR*). The ubiquitously-expressed *armadillo-Gal4* (*arm>*) driver was used to drive *UAS-darhgef10-IR* thoughout the life of the flies. A - males; B - females. *arm>* and *UAS-darhgef10-IR* flies were crossed with *w[1118]* flies as controls. Curves with asterisks are statistically significantly different at $\alpha = 0.017$, according to the log rank test (http://bioinf.wehi.edu.au/software/russell/logrank/). The color of the asterisks is relative to the color of the control curve that *arm>darhgef10* longevity is statistically significant. $N_{arm>darhgef10\text{-}IR}$= 61 (male), 93 (female); $N_{arm>}$= 68 (male), 92(female); $N_{UAS\text{-}darhgef10\text{-}IR}$= 74 (male), 76 (female).

The results indicate that the lifespan of *arm>darhgef10-IR* male flies was not increased relative to the controls. Female *arm>darhgef10-IR* flies had a shorter or longer lifespan, depending on the control used for the comparison (Figure 22).

Therefore, it is difficult to conclude whether or not ubiquitous knock-down of d*arhgef10* leads to an increased lifespan, so these experiments do not provide independent evidence supporting the conclusion that the increased longevity observed in *darhgef10* mutant male flies is due to *darhgef10* mutations. Notwithstanding, we must consider the possibility that the observed results would arise from leaky RNAi expression originating from the control *UAS-darhgef10-IR*. To test this, we could check the heart of these flies to look for misaligned cardioblasts or perform a qRT-PCR to analyze the transcript levels of *darhgef10*. Nevertheless, if there was already RNAi expression, it would be difficult to explain why these flies live more than the ones where we are ubiquitously expressing *darhgef10*-IR. If the observed results are due to the genetic background of the RNAi line, we can add a new control in this assay with, such as, RNAi against GFP of the same RNAi library (KK library). Taken our longevity results together it is unlikely that the effect in longevity observed in *darhgef10* flies is specifically due to the deletion of the gene in study.

3.1.4 Negative geotaxis behavior assay

To investigate whether the heart defect of *darhgef10* mutants could affect locomotor behavior, we analyzed the capacity of *darhgef10* mutant flies to maintain their negative geotaxis behavior during their adult lifespan.

Surprisingly, *darhgef10* mutant flies did not have a reduced negative geotaxis response relative to control *w[1118]* flies. Instead, there was a tendency which sometimes reached statistical significance (e.g., $p < 0.017$ for *Df(1)ΔB* flies at the age of 40 d after adult eclosion) for *darhgef10* mutant flies to climb greater heights than the control flies (Figure 23). This effect is most clearly visualized by plotting the percentage of flies that have reached a height above 6 cm throughout time (Figure 24). Indeed, starting at 20 d of age, the percentage of mutant flies climbing >6 cm is always superior than the controls. Even at 60 d, approximately 20% of the *Df(1)ΔB* flies climbed at least 6 cm.

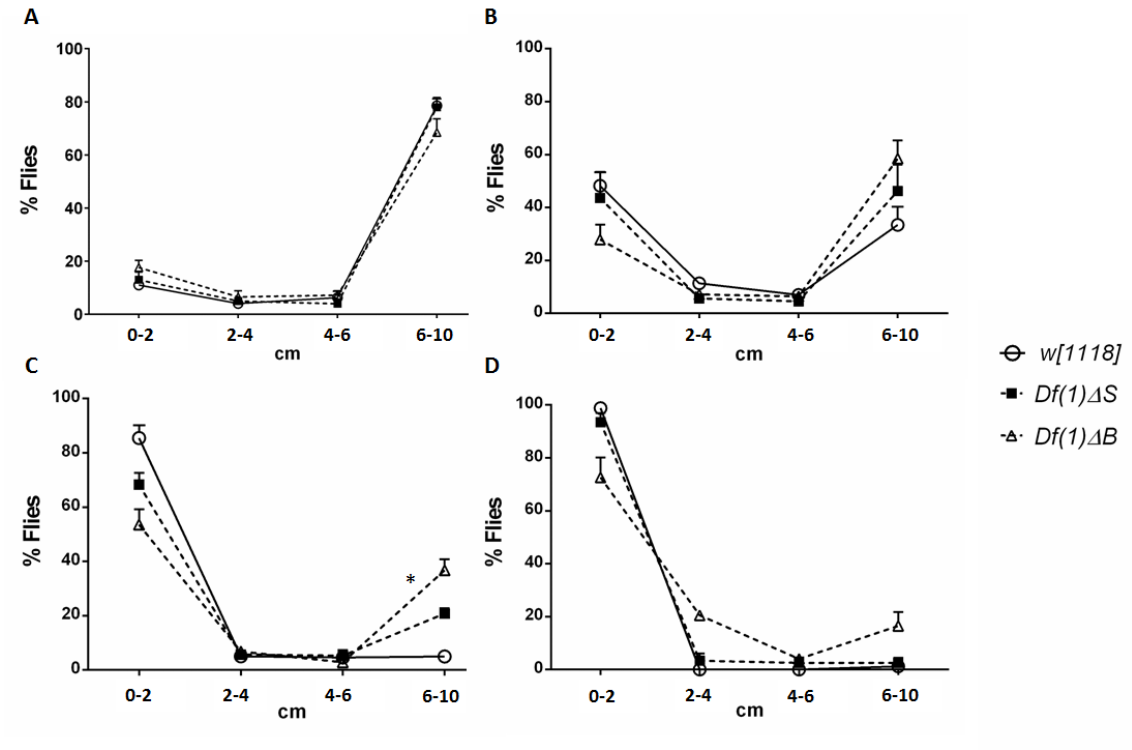

Figure 23 – Negative geotaxis behavior of *darhgef10* mutants and *white[1118]* control male adult flies aged: A - 24 h after adult eclosion (AAE), B - 20 d AAE, C - 40 d AAE and D - 60 d AAE. Graphs represent the percentage of flies (y axis) that were in the interval of height in cm (x axis), 10 s after the start of the assay (see 2.2.3). Error bars represent the standard error of the mean (SEM). Curves with an asterisk are statistically significantly different from the others at α = 0.017, according to the Fisher's test followed by Bonferroni correction for multiple comparisons.

With these results, we conclude that *darhgef10* flies have either a normal or improved locomotor capacity relative to control flies. These findings are again surprising considering that *darhgef10* flies develop with an abnormal heart. However, the normal or slightly improved locomotor capacity is consistent with the normal or slightly extended lifespan of flies lacking *darhgef10*. Therefore, even though *darhgef10* is critical for proper heart development and full viability during development, it appears dispensable for many aspects of adult life in normal laboratory conditions.

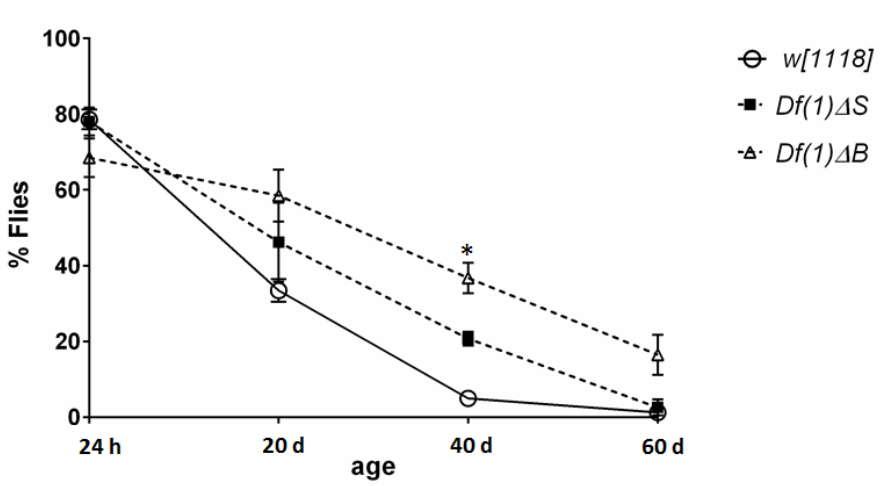

Figure 24 - Full anti-gravitational response of *darhgef10* mutant male flies and *w[1118]* (control). Graph represents the percentage of flies at different ages that climbed more than 6 cm in the assay. This is a summary of the corresponding data presented on Figure 6. See Figure 6 for statistical analyses. The sole point that was statistically different between the genotypes in the previous analyses is indicated with an asterisk. Error bars represent SEM.

3.2 Expression localization expression patterns

In order to access the cellular localization of dArhgef10, a set of rat polyclonal antibodies (PABs) were generated against a His-tagged-113-aa fragment corresponding to aa 700 to 813 of the dArhgef10 protein (Metabion). In total, 4 rats were injected resulting in 4 different immune serums, here termed as anti-dArhgef10 antibody #1, #2, #3 and #4. Unfortunately, in immunohistochemistry assay, none of the PABs gave any detectable unique signal in *w[1118]* control embryos when compared to *Df(1)ΔB* protein null embryos. Therefore, we were neither able to independently confirm the cardioblast enrichment or to gain insight into the intracellular distribution of dArhgef10 using this strategy alone.

3.2.1 *darhgef10* overexpression *in vitro*

To test the PABs in a technique where dArhgef10 epitopes are more accessible for antibody binding, we performed Western blot, using lysates from S2 cells, overexpressing or not *darhgef10* using the Gal4-UAS system. For this, Gal4 was constitutively provided by transfecting the cells with a plasmid containing an Act-Gal4 sequence. These cells were co-transfected with *pTw::darhgef10* or *pTGw::darhgef10*, which drive wild-type dArhgef10 or a GFP::dArhgef10 translational fusion. An empty *pUAST* vector served as control for equimolar transfections (*pUAST-empty)*.

In contrast to the immunofluorescence assays in embryos, three out of the 4 PABs (annexes Figure II) gave a positive result in the Western blots. PAB#1 produced no detectable specific signal. PABs#2-4 clearly detected a 158-KDa band migrating at the expected size for dArhgef10. While PABs #3 and #4 gave the least background and strongest signal. Interestingly, PABs#2-4 only recognized dArhgef10 in the cell lysates where dArhgef10 was overexpressed without the GFP tag. As this was a bit unexpected since the epitope against which the PABs were raised is far from the C-terminal end where the GFP tag is fused, we repeated the transfections with new plasmid preps and also performed parallel immunofluorescence assays with the transfected cells in order to check if the GFP::dArhgef10 construct was functioning as expected (*i.e.*, producing green fluorescence).

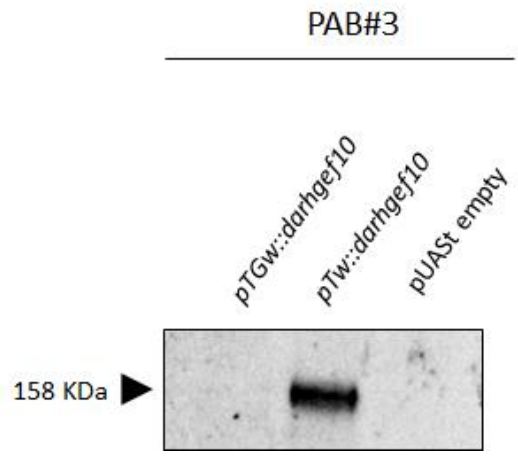

Figure 25 - Western blot analysis of *darhgef10* overexpression in S2 cells transfected with a *pTGw::darhgef10* plasmid for overexpression of *darhgef10* marked with GFP, with a *pTw::darhgef10* plasmid for overexpression of untagged *darhgef10* and with a *pUAST*-empty plasmid to serve as a control. PAB#3 was chosen as an example, the same assay was performed with PAB#4, with similar results (see full membrane in annexes figure III).

Consistent with the previous experiments, only the cell lysates from S2 cells transfected with *pTw::darhgef10*, which encodes the wild-type untagged dArhgef10 produced a detectable band in Western blot analyses using anti-dArhgef10 PABs (PAB#3; Figure 25). Cells transfected with *pTGw::darhgef10*, which encodes the GFP::dArhgef10 fusion, was again not detected by the same PABs. By looking at the cells processed in parallel for immunofluorescence analyses, we could also only detect positive anti-dArgef10 signals in cells transfected with the *pTw::darhgef10* plasmid coding untagged dArhgef10 (Figure 26). In contrast, no anti-dArhgef10 signal was obtained from cells transfected with *pTGw::darhgef10* encoding GFP::dArhgef10, although we could clearly see GFP expression enriched in membrane compartments. Therefore, we conclude that the *pTGw::darhgef10* construct is functional, but the GFP tag leads to the masking of the anti-dArhgef10 epitope. As this masking is retained in Western blot analyses of proteins under denaturing conditions, the masking must be due to post-translational modification of the GFP::dArhgef10 protein, such as a covalently linked post-translational modification or some type of processing of the protein that removes or masks the epitope. It is unclear if this finding could provide any hint towards the biology of dArhgef10.

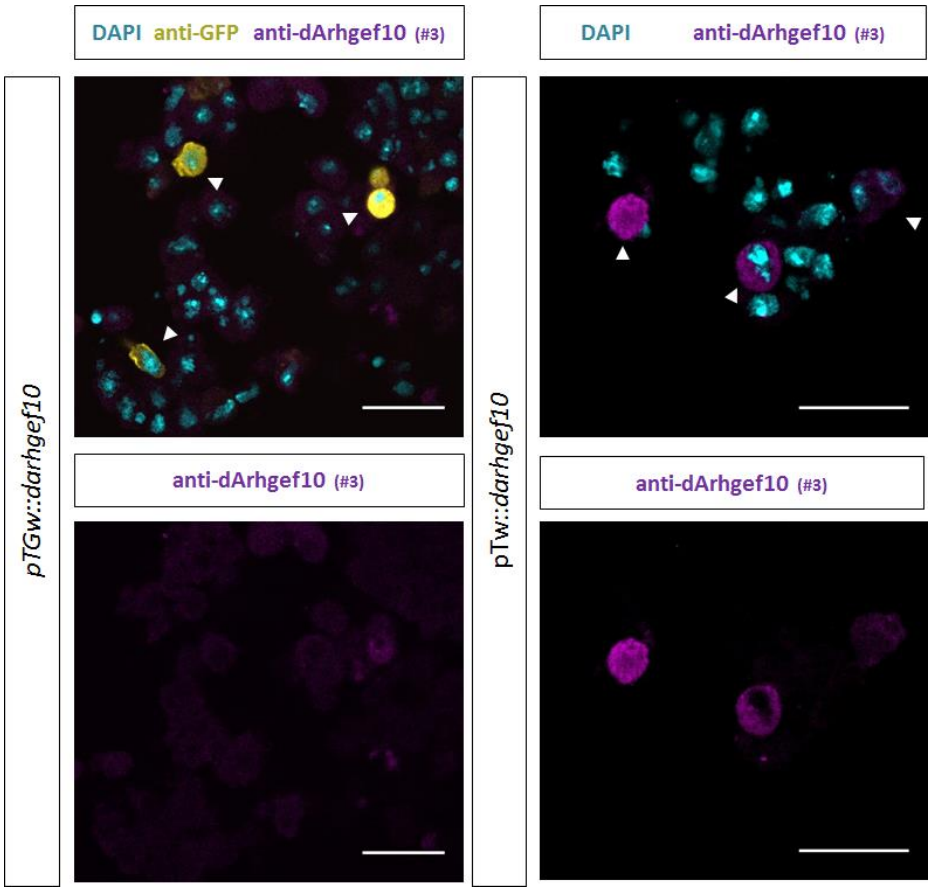

Figure 26 – S2 cells transfected with *pTGw::darhgef10* (left) and *pTw::darhgef10* (right), which encode GFP::dArhgef10 and untagged dArhgef10, respectively. Arrowheads indicate the transfected cells. PAB#3 was chosen as an example, but the same assay was performed with PAB#4, with similar results. Cyan, DAPI counterstain. Yellow, anti-GFP. Magenta, anti-dArhgef10 (PAB#3). Scale bar: 20 µm.

Our immunofluorescence analyses revealed that dArhgef10 is a cytosolic protein slightly enriched in the cellular membranes (Figures 26-28). Despite the overexpressed dArhgef10 having the same expected molecular weight as the endogenous dArhgef10, thus suggesting that *pTw::darhgef10* construct is correctly coding a functional dArhgef10 protein, we are observing GFP::dArhgef10 in an overexpression context, therefore caution is warranted in interpreting this pattern as the pattern of the endogenous protein.

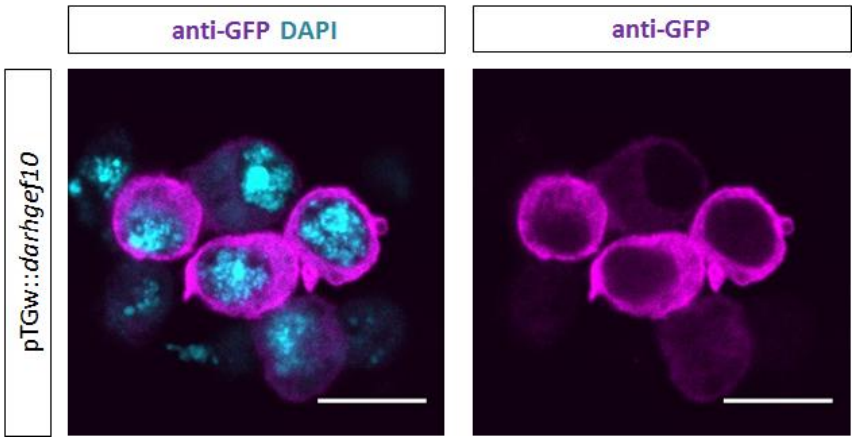

Figure 27 – S2 cells transfected with *pTGw::darhgef10*, which encodes GFP::dArhgef10. Right panel is a maximum intensity projection of all z-confocal stacks. Magenta, anti-GFP. Cyan, DAPI counterstain. Scale bar: 10 µm.

Unfortunately, we were unable to detect a clear signal in the non-transfected cells either by immunofluorescence or by Western blot, which would correspond to the endogenous dArhgef10. These results could indicate that dArhgef10 is normally not expressed in *Drosophila* S2 cells or alternatively that its expression levels are extremely low.

In humans, ARHGEF10 is a specific activator of RhoA(Aoki *et al.*, 2009; Chaya *et al.*, 2011), the human homolog of Rho1. To verify if dArhgef10 and Rho1 co-localized in *Drosophila*, we performed immunofluoresence assays of S2 cells transfected with *pTGw::darhgef10*, which encodes the GFP::dArhgef10 fusion protein, and looked for Rho1 using a mouse monoclonal antibody against Rho1 (anti-Rho1). We indeed found accumulation of dArhgef10 in membrane protrusions, associated with F-actin and the RhoGTPase Rho1 (Figure 28). Thus, it is likely that dArhgef10 acts similarly to human ARHGEF10, by nucleating and activating Rho1, which would then mediate the reorganization of actin cytoskeleton by actin turnover and polymerization. The membrane protrusions observed in these fixed cells could be linked to filopodia formation and cell migration.

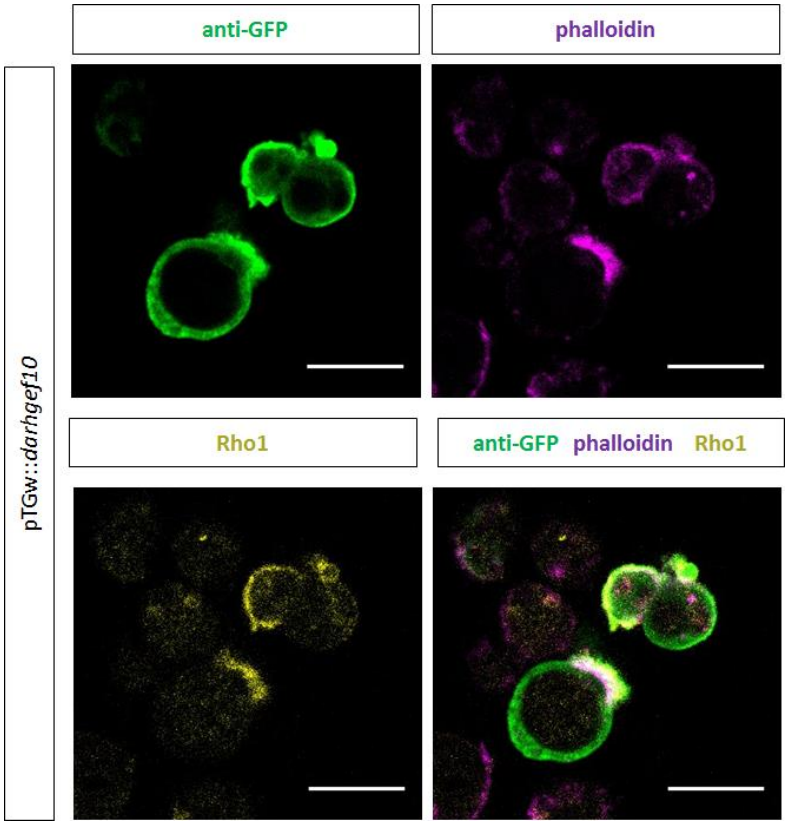

Figure 28 - Confocal sections of fixed S2 cells previously transfected with *pTGw::darhgef10* plasmid, which encodes a GFP::dArhgef10 fusion protein. Anti-GFP, green. Phalloidin (for F-Actin), magenta. Anti-Rho1, yellow. Scale bars: 10 µm.

In future experiments we could test for a role of dArhgef10 in actin cytoskeleton organization and in cell migration, using live imaging of cells co-transfected with *pTGW::darhgef10* and a *pUASP-mCherry::moesin* construct. Moesin is a member of the ERM (Ezrin, Radixin, Moesin) protein family (Fehon, McClatchey and Bretscher, 2010), which cross-links the plasma membrane and the underlying actin cytoskeleton. Moesin is localized to developing filopodia, thus being an efficient reporter for changes in the actin cytoskeleton. Hopefully, this way we could better understand the effects caused by ectopic dArhgef10 expression.

3.2.2 *darhgef10* overexpression *in vivo*

In order to observe the subcellular distribution of dArhgef10 and the cellular effects caused by its ectopic overexpression *in vivo*, we made transgenic flies carrying the Gal4-inducible construct *pTw::darhgef10*. Expression of this construct in muscle using the *mef-2-Gal4* (Lilly *et al.*, 1995) driver was lethal. In order to be able to observe the subcellular effects more clearly we chose to target non-essential tissues and also tissues with large cells. The *eyless-Gal4* driver (*ey>*) is expressed in the eye field of eye-antennal imaginal discs and in salivary glands (Quiring *et al.*, 1994), both of which are non-essential structures and the latter of which has very large cells, facilitating studies of subcellular localization.

We thus crossed *ey>* and *pTw::darhgef10* animals and dissected salivary glands of the *ey>pTw::darhgef10* (hereafter *ey>darhgef10*) L1 larvae for immunofluorescence analyses. F-actin and dArhgef10 were detected with phalloidin and anti-dArhgef10, respectively. We found that *darhgef10* overexpression in salivary glands disrupts its normal morphology (Figure 29). Abnormal glands are substantially smaller than the control ones (*w[1118]*) and some of them are swollen, presenting a large number of what appear to be vesicles mainly in the basal surface. Additionally, dArhgef10 overexpression seems to lead to an accumulation and abnormal organization of F-actin (Figure 29). Anti-dArhgef10 staining is detected associated with the F-actin accumulations, as occurs during ectopic expression of dArhgef10 in S2 cells. The anti-dArhgef10 staining seems to preferentially accumulate in the basal surface of the salivary gland (Figure 30).

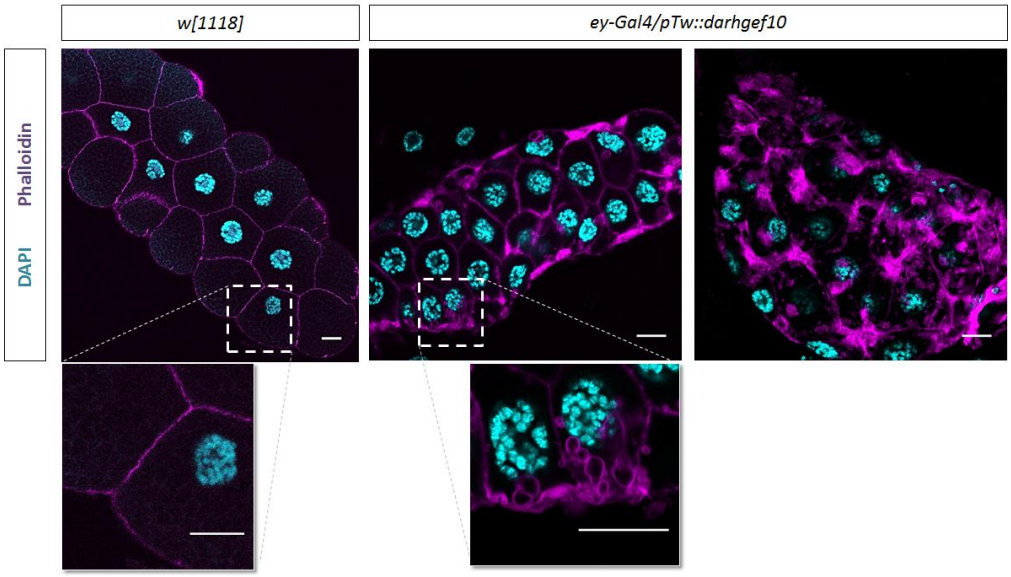

Figure 29 – Confocal section of salivary glands from control (*w[1118]*) or *ey>darhgef10* (*ey-Gal4/pTw::darhgef10*) L3 larvae. Salivary glands are stained with phalloidin for F-actin (magenta) and counterstained with DAPI (blue). Scale bar: 20 µm.

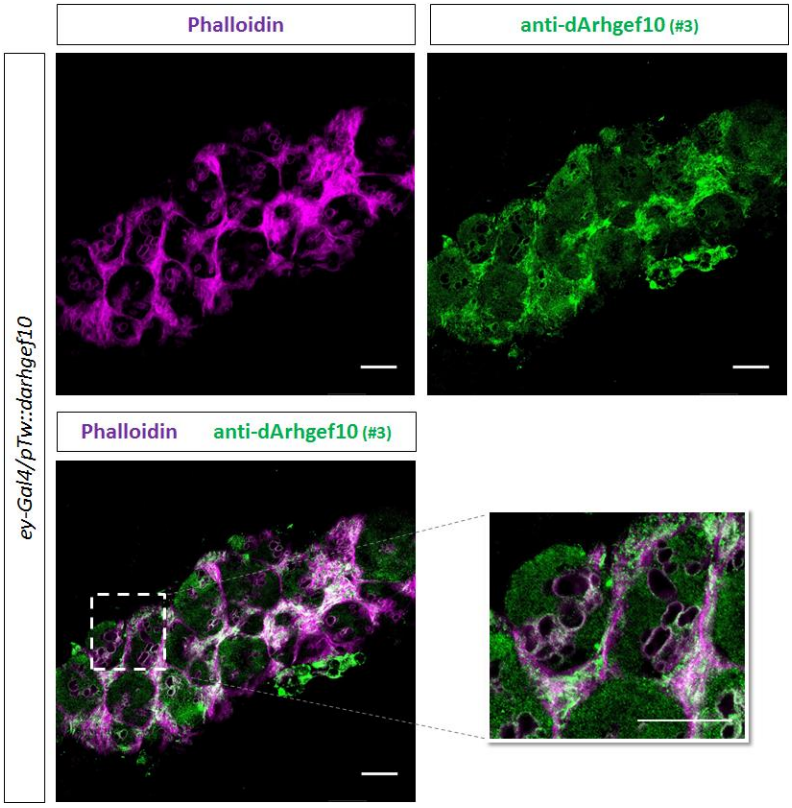

Figure 30 – Confocal section of salivary glands from *ey>darhgef10* (*ey-Gal4/pTw::darhgef10*) L3 larvae. Salivary glands are stained with phalloidin for F-actin (magenta) and anti-dArhgef10 (green). Scale bar: 20 µm.

3.2.3 Targeted genome editing using CRISPR-Cas9 for endogenous dArhgef10 detection

We have generated functional dArhgef10 antibodies capable of detecting overexpressed dArhgef10 in cell culture or *in vivo*, both by Western blot and immunohistochemistry. However, we were unable to unequivocally identify any specific staining that would correspond to endogenously expressed dArhgef10 protein. In order to gain insight into the endogenous expression pattern of dArhgef10 protein, we attempted to use CRISPR-Cas9-mediated homologous recombination repair to insert an *OLLAS-tagged superfolder GFP* (*sfGFP*) immediately before the stop codon of the endogenous *darhgef10*, so we would have all potential *darhgef10* isoforms labelled *in vivo*. The sfGFP::OLLAS cassette would be separated from the dArhgef10 by a small flexible Glycine-Serine-rich polylinker sequence to facilitate the folding of the protein domains.

As described in 2.3.2, we used two set of primers (Figure 31) to check for the insertion of the repair cassette in the fly genome. The number of viable and fertile flies originating from CRISPR-Cas9 injection was very low: from the injection of more than 200 embryos, and then ~120 larvae, only 15 adults hatched, accounting for less than 10% survival, with the major lethality observed in the transition from larvae to pupae. We were only able to screen by PCR 50 potential transformants from these flies for the correct homologous recombination repair event, but unfortunately none were positive for the PCR product with either primer pair 1 or 2 (Figure 31). We also confirmed this negative result by using a combination of primers in the *darhgef10* region (black arrows in Figure 31) and obtained a PCR product of the size expected for this *darhgef10* region without any cassette insertion. Together, these results showed that we were unable to edit the *darhgef10* locus using this specific CRISPR-Cas9 strategy.

Figure 31 – Scheme used to screen flies and S2 cells for successful homologous recombination repair. PCR product of Pair 1 is 975 bp, Pair 2 and Pair 3 is 587 bp.

One of the most common reasons why CRISPR-Cas9 does not work is that the guideRNA used does not lead to efficient cutting by Cas9 at the target locus. To test whether the guideRNA we used was able to mediate homologous recombination repair we tested the whole system in S2 cells by co-transfecting the same plasmids used for the embryo injections [*arhgef10::sfGFP::OLLAS* repair cassette (in the *pUC57* plasmid) and the *darhgef10* guideRNA (in the *pU6-BbsI-chiRNA* plasmid)] plus an additional *pAc-sgRNA-Cas9* plasmid for constitutive *cas9* expression in the *Drosophila* cells. We extracted DNA from the cells and performed PCR using primer pair 1 and pair 2 (Figure 32).

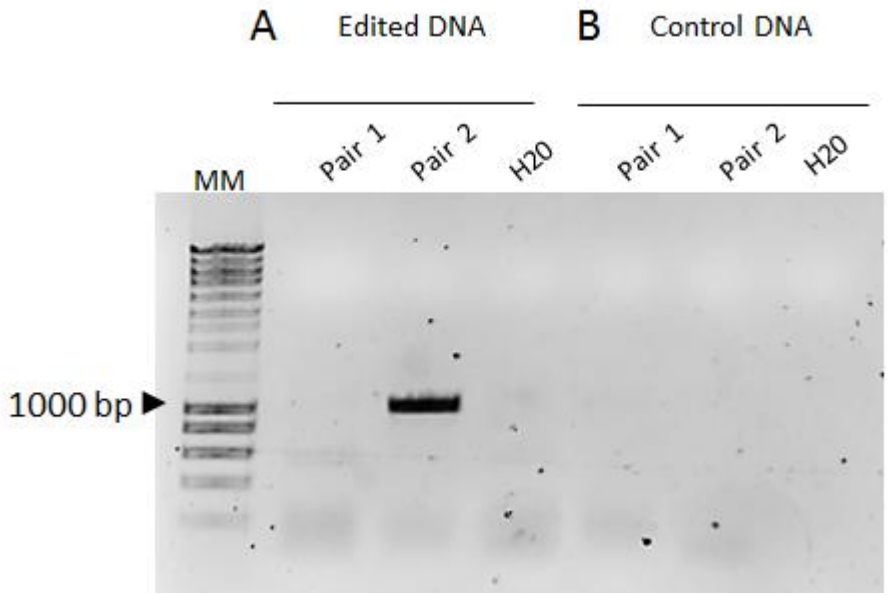

Figure 32 - Analysis of PCR products in agarose gel of genome amplification of S2 cells transfected with: A - repair cassette into pUC57 plasmid, guideRNA into pU6-BbsI-chiRNA and pAc-sgRNA-Cas9 plasmid for cas9 expression; B - repair cassette into pUC57 plasmid, pU6-BbsI-chiRNA empty and pAc-sgRNA-Cas9 plasmid for cas9 expression. DNA volume was replaced with H_20 in control reaction.

While primer pair 2 produced a PCR product of the expected size, indicating correct insertion of the repair cassette into the genome, the primer pair 1 did not show any amplification. To test if this was a problem with the primer pairs and not with the insertion, we test a new set of primers for this region, primer pair 3, and it amplified a product consistent with the correct insertion (Figure 33). We conclude that the

guideRNA used in our CRISPR-Cas9 strategy is able to recognize the matching genome sequence to allow homologous recombination repair.

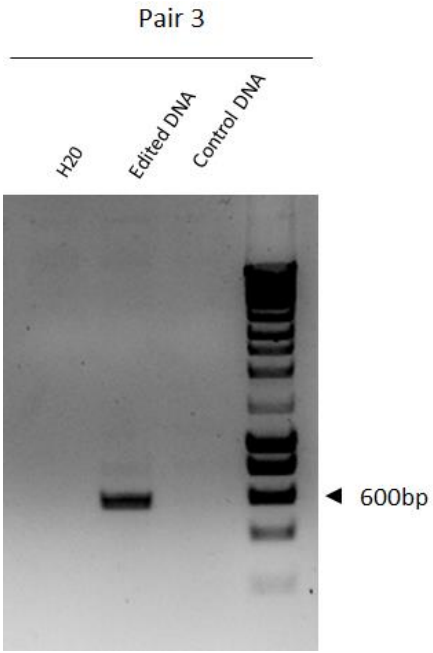

Figure 33 - Analysis of PCR products amplified with primer pair 3 in agarose gel of genome amplification of S2 cells transfected with repair cassette into pUC57 plasmid, guideRNA into pU6-BbsI-chiRNA and pAc-sgRNA-Cas9 plasmid for cas9 expression - edited DNA; repair cassette into pUC57 plasmid, pU6-BbsI-chiRNA empty and pAc-sgRNA-Cas9 plasmid for cas9 expression – Control DNA. DNA volume was replaced with H_20 in control reaction.

Possible explanations for the unsuccessfully fly genome editing could be related with chromatin conformation or interference with regulatory regions. A high condensation level of chromatin could prevent Cas9 to get in the target region, for instance. This hypothesis is not rejected by the S2 cells result, since the chromatin architecture of *Drosophila* cells *in vivo* and *in vitro* could be different. Another point to consider is the high lethality of the CRISPR-Cas9 injection. This led us to consider the possibility that the successful homologous recombination repair events (insertion of the GFP downstream of the dArhgef10 were somehow leading to lethality). We were not expecting lethality in this injection as both *darhgef10* deletions *(Df(1)ΔB* and *Df(1)ΔS)* are homozygous viable. Yet, as we have shown above, *darhgef10* gain of function by means of ectopic expression, is highly toxic to tissues and causes lethality when

expressed in muscles, for instance. Therefore, it is possible that the repair cassette insertion interferes with endogenous dArhgef10 activity, leading to a gain-of-function phenotype. Interestingly, while we readily obtain *pTw::darhgef10* transformants, we were unable to obtain a *pTGw::darhgef10* transformant, which would encode the UAS-driven GFP-tagged dArhgef10. One of the possibilities is that the *pTw* and *pTGw* constructs are a little leaky without Gal4, and while the untagged dArhgef10 version does no large harm to the cells, the GFP-tagged dArhgef10 is highly toxic.

Two possibilities to overcome this problem is to insert the GFP N-terminally to dArhgef10 or at another site of the protein. The problem with the N-terminal insertion is that we have to choose one single isoform, as there are different *darhgef10* transcripts with different start codons. The other option is to make the CRISPR-Cas9 injections in a background where *darhgef10* is constitutively knocked-down by RNAi. This is feasible because broad RNAi against *darhgef10* does not strongly compromise viability and fertility. A temperature sensitive *tub-Gal80* (*tub-Gal80ts*) cassette, which would inhibit the RNAi, could be included to allow temperature dependent expression of the endogenously-tagged dArhgef10::GFP::OLLAS, by transiently eliminating the RNAi during the temperature shifts.

3.3 Cell biology and the dArhgef10 pathway

As described in 1.2, dorsal vessel development is dependent on the formation and maturation of a series of stable adhesions between the cardioblasts. To start investigating if dArhgef10 is involved in the formation and/or maturation of these long-term adhesions, we looked at the expression of key components of the Integrin Adhesion Complex (IAC). Our aim is to bring new insights into the dArhgef10 pathway and understand the nature of the cellular defect leading to the misaligned cardioblasts phenotype of *darhgef10* mutants.

3.3.1 dArhgef10 in heart development

To verify if dArhgef10 played any role in regulating cellular adhesion during dorsal vessel development, we looked at the expression of key proteins required for the cell-cell and extracellular matrix cell adhesion, namely Talin and βPS integrin proteins, by immunofluorescence analyses of *darhgef10* mutant stage 16 embryos, immediately before the heart starts to beat (Figure 34).

Talin is mainly expressed in muscle attachment sites and faintly in the dorsal vessel, while integrin is expressed either in muscle attachment sites (see figure 34) and dorsal vessel, for cardioblasts adherence. We did not see any relevant difference between the expression or localization of Talin, nor of βPS integrin between the control *w[1118]* and *darhgef10* mutants. Only *Df(1)ΔB* embryos are shown in figure 34 but we obtained the same results with *Df(1)ΔS* embryos.

To test the hypothesis that *darhgef10* affects muscle cell migration we performed live imaging confocal microscopy during cardioblasts alignment and migration to the dorsal midline where they will give origin to the dorsal vessel. We used the *darhgef10[Df(1)ΔB];;UAS-lifeactGFP,Mef2Gal4/TM6b* and the *darhgef10[Df(1)ΔS];;UAS-lifeactGFP,Mef2Gal4/TM6b* reporter lines to visualize the actin cytoskeleton in *darhgef10* mutants. Our main aim in this assay is to study the cellular basis of the cardioblasts defect. Live imaging of embryos was performed until

the dorsal vessel was formed, which is coincident with the dorsal closure event (figure 35).

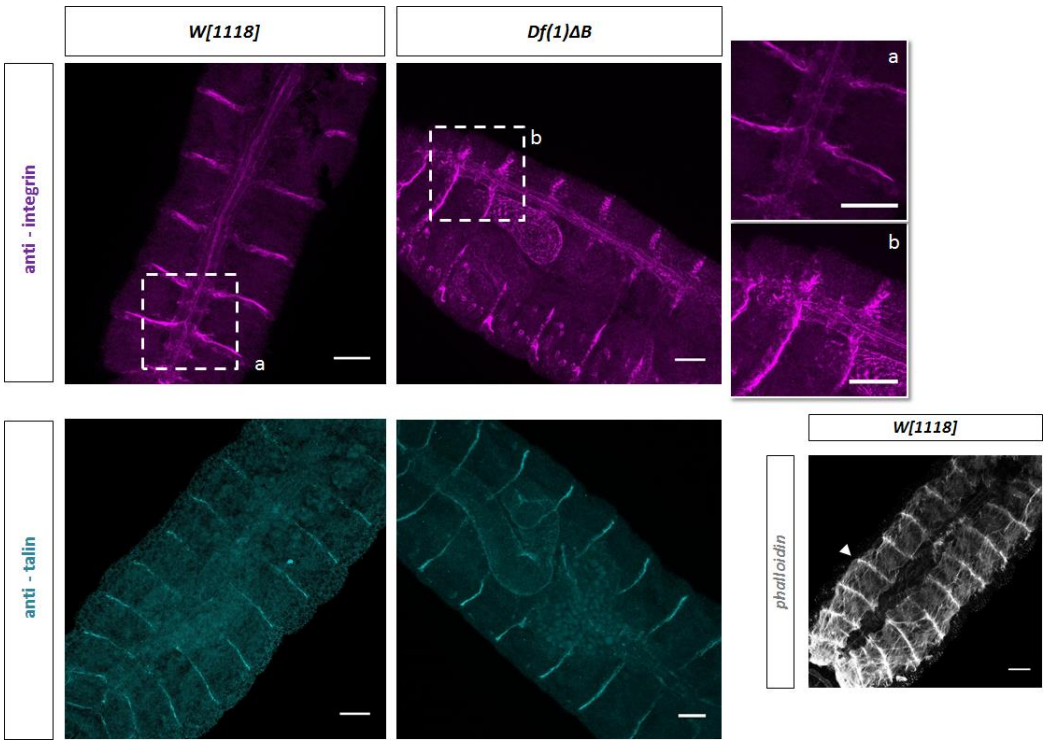

Figure 34 – Confocal images of Talin and βPS integrin expression detected by immunofluorescence analysis of stage 16 embryos from *darhgef10* mutants and *w[1118]* controls. Muscle staining in *w[1118]* stage 16 embryo (right bottom). Arrowhead indicates muscle attachments sites. Scale bars: 20 µm.

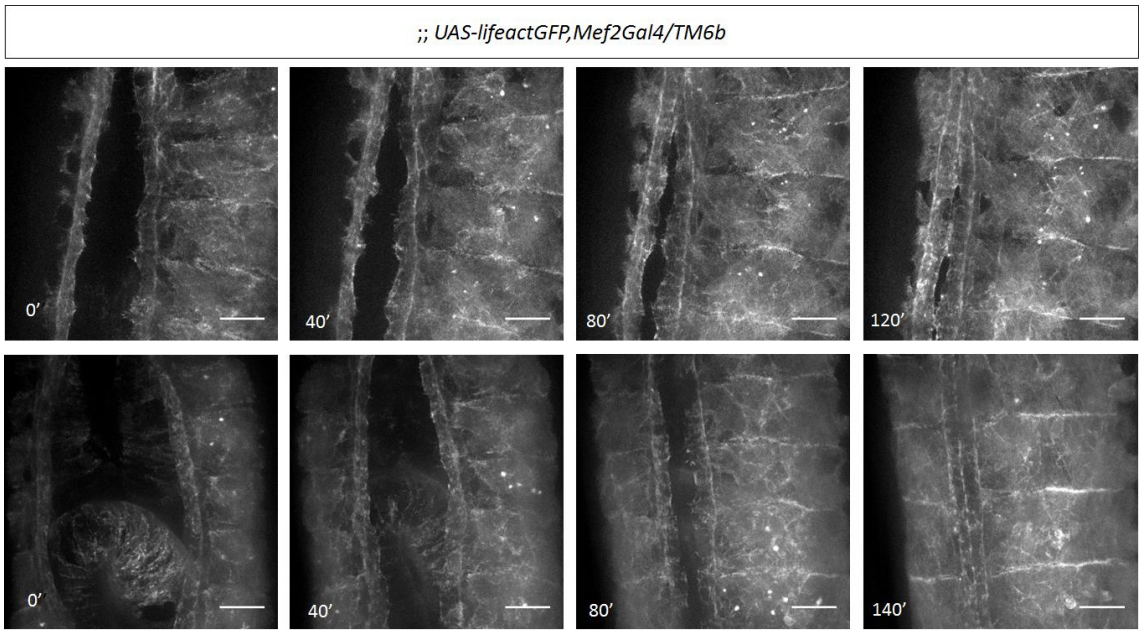

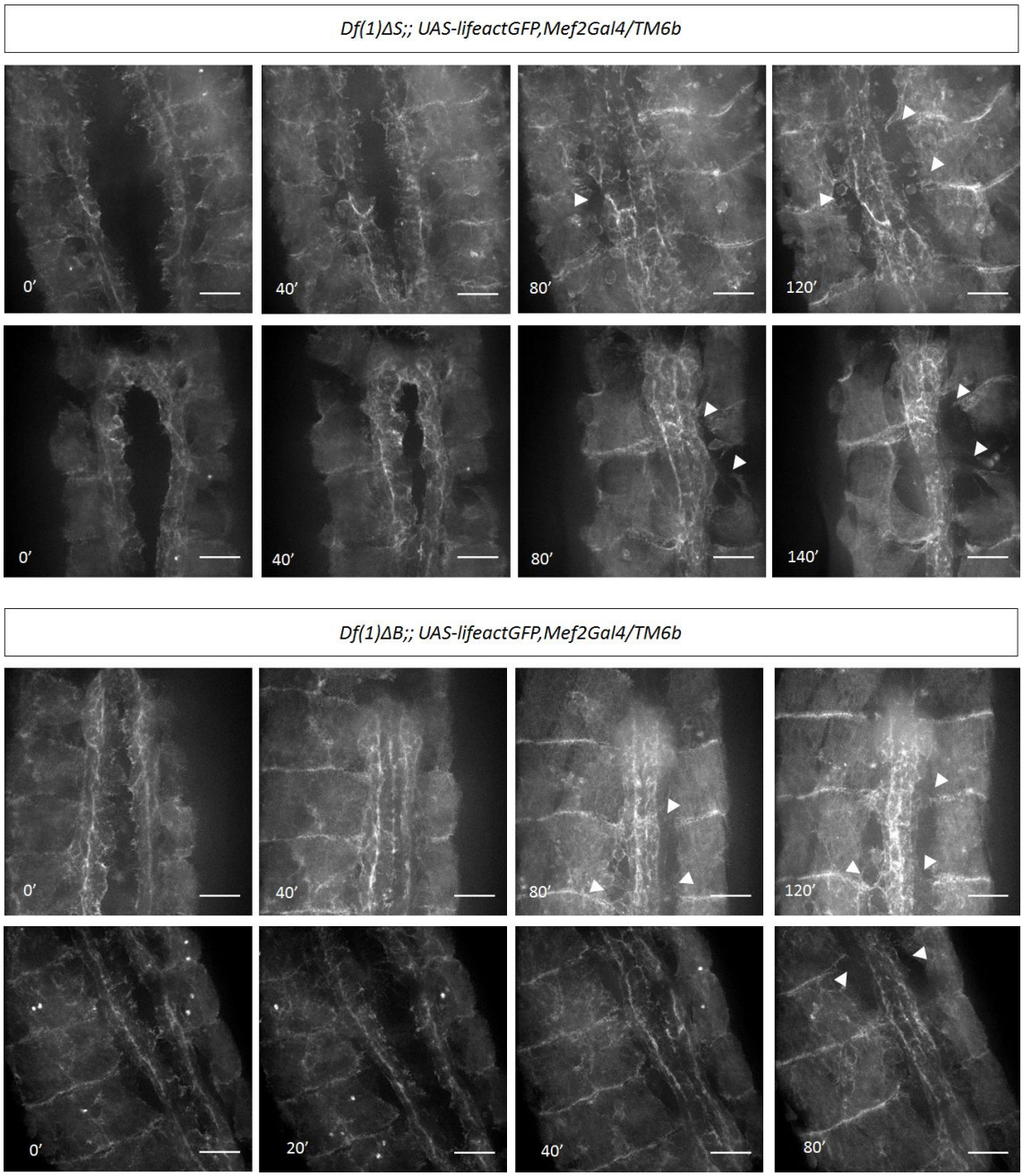

Figure 35 – Live imaging of the dorsal vessel development in control (*w[1118]*) and *darhgef10* mutant embryos. Projection of z-stacks obtained using spinning disc imaging. Arrowheads indicate the dorsal vessel defect found in *darhgef10* embryos. Scale bars: 20 µm.

Live imaging of actin filaments in *mef2* cells during dorsal vessel development reveals a pronounced defect in *darhgef10* mutant embryos. We observed larger than expected actin-poor regions adjacent to the dorsal vessel, where either body wall muscle and/or alary muscles are positioned in wild-type embryos (see arrowheads in figure 35). The cellular basis of the observed defect (Figure 9) and its relationship to the misaligned cardioblast phenotype are not yet clear and will be the focus of further work. One possibility is that this reflects some defective attachment of alary muscles and/or pericardial cells to the dorsal vessel. Alary muscles normally attach to pericardial cells, which do not express high levels of *darhgef10* (Mantas Dias, 2012). So, we hypothesize that *darhgef10* is required for the correct interaction between cardioblasts and pericardial cells. Our preliminary impression is that this loss of adhesion event occurs more frequently during the final stages of embryonic dorsal vessel development, when the counterlateral rows of cardioblasts meet each other at the dorsal midline, to form the cardiac tube. To independently confirm this observation, we need to perform additional live imaging studies of control and *darhgef10* mutant embryos and devise methods to quantify this phenotype. In parallel, we would use specific cardiac cellular reporters as *hand-Gal4* (*hand>*; drives expression specifically in cardioblasts and pericardial cells), and the alary muscle reporter *org-1-SM-RFP* (Han *et al.*, 2006; Hollfelder, Frasch and Reim, 2014). We can still look for this phenotype in *darhgef10-IR;UAS-lifeactGFP,Mef2Gal4/TM6b* embryos to conclude if it is a phenotype caused specifically by lack of *darhgef10*.

3.3.2 Genetic interaction between dArhgef10 and candidate effectors

Next, we looked for genes that could suppress or enhance the eye malformation caused by ectopic expression of *darhgef10* in the developing eye. Our main objective was to find dArhgef10 effectors. For this, we reduced the activity, by mutation or RNAi respectively, of either the *Drosophila RHOA*-homologue, *Rho1* or its primary effector proteins, the *ROCK-like Rho-kinase* (*Rok*) and the *DIAPH1*-homologue *diaphanous* (*dia*) genes, any of which could mediate dArhgef10 activity (Figure 6). As proof of principle for our strategy we reduced *darhgef10* activity using *darhgef10*-IR and registered a complete suppression of the *ey>darhgef10* eye malformation phenotype

(Figure 36). This reassured us that the eye deformation is caused by *darhgef10* overexpression at the same time that it demonstrated the reliability of this RNAi line for *darhgef10*.

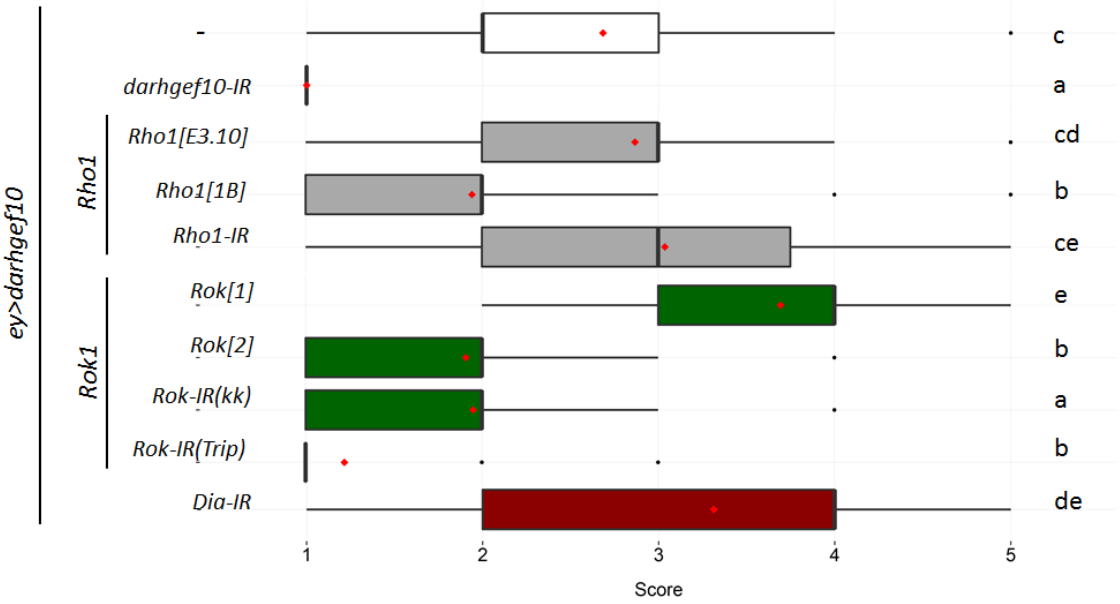

Figure 36 - Box and whiskers plot showing the interaction between dArhgef10 and candidate effectors. Plotted is the phenotypic score of the eye malformation caused by *ey>darhgef10*, which goes from 1 (wild-type eye) to 5 (severe malformation) - see Figure 14. Red dots represent averages, dark bars represent medians and black dots are outliers. Groups sharing the same letters are not statistically significant at $\alpha = 0.05$, according to the Tuckey's HSD post-hoc test. N = 60, 92, 40, 88, 26, 38, 68, 100, 82 and 64, respectively, for the genotypes depicted from top to bottom.

We were able to test two different mutant alleles for *Rok*, *Rok[1]* and *[2]*, and two independent RNAi lines (*Rok-IR*) from the phC31 RNAi library (KK) and Transgenic RNAi Project (TRiP) library (Dietzl *et al.*, 2007; Ni *et al.*, 2008). Both *Rok-IR* lines statistically significantly improved the *ey>darhgef10* eye malformation, with the *Rok-IR-TRIP* construct giving a complete suppression of the phenotype. Likewise, halving the dosage *Rok* by crossing the *Rok[2]* allele into a *ey>darhgef10* background also statistically significantly ammeliorated the eye malformation phenotype. An identical experiment using a second *Rok* allele, *Rok[1]*, gave the opposite phenotype,

with a statistically significant enhancement of the *darhgef10*-dependent eye malformation phenotype.

Even though *Rok[1]* did not suppress the eye phenotype caused by *darhgef10* overexpression, the fact that the other allele, *Rok[2]* and two independent RNAi lines did, suggests that *Rok* encodes a gene required for the dArhgef10-dependent activity that interferes with normal eye formation. While *Rok[2]* is clearly a strong loss-of-function mutation, with a G to A substitution at the 3'end of intron 1, the molecular nature of *Rok[1]* has not yet been determined (Winter *et al.*, 2001). In the original paper isolating both *Rok* alleles, it is evident that both *Rok[1]* and *Rok[2]* are equally strong mutations in *Rok.* Both eliminate the *Rok* activity required for embryonic viability and are rescuable by a transgenically-provided *Rok*. How then could we reconcile these findings with the opposite effects these alleles had on our eye deformation assay? One possibility is that, as the molecular nature of the *Rok[1]* allele has not yet been defined, it could well be a regulatory mutation that eliminates *Rok* transcripts from critical embryonic tissues but retains wild-type or ectopic *Rok* in certain tissues in later stages of development, such as in the eye discs during larval development.

Our results with Rho1 were surprising and did not directly fit the expected model from the literature based on human ARHGEF10 and RhoA (Chaya *et al.*, 2011), and what we were expecting based on our S2 cell results, where Rho1 looks closely spatially-associated with ectopically-provided dArhgef10 (Figure 28). Here, we found that reducing *Rho1* activity by half using the *Rho1[1B]* allele (Magie and Parkhurst, 2005) partially-rescued the *ey>darhgef10* phenotype, doing the same with the *Rho1* allele *Rho1[E3.10]* (Halsell, Chu and Kiehart, 2000) or reducing *Rho1* function with the *Rho1* RNAi line, *Rho1-IR*, had no effect on the *ey>darhgef10* phenotype. We have no reason to think *Rho1[1B]* and *Rho1[E3.10]* are not both equally strong loss-of-function alleles for *Rho1*. Thus, with these contradictory results, we are obliged to consider the possibility that dArhgef10 might not be acting via Rho1, at least in this context. The less likely scenario is that *Rho1[E3.10]* differs in a very particular aspect from *Rho1[1B]* allele and the *Rho1-IR* is not functional.

The fact that Drosophila Rok is clearly required for dArhgef10 activity, is likewise puzzling because Rok/ROCK is considered to have Rho1 GTPase as its main or sole activator (Winter *et al.*, 2001). To reconcile these data, dArhgef10 would have to

stimulate Rok activity in a Rho1-independent manner. For instance, dArhgef10 could activate another phylogenetically-related member of the Drosophila RhoA clade, which would then mediate Rok activation. A possible candidate would be the Rho1-like molecule, the Rho-Like protein, RhoL, which is highly conserved in animals, but has apparently been lost in human.

The other Rho1 effector assayed, Diaphanous, statistically significantly enhanced the *ey>darhgef10* phenotype when reduced by RNAi (Figure 36). Unfortunately we were only able use one condition to reduce *dia* function. It will be important to re-test this with an independent RNAi and with mutations.

Our initial aim was to use myocyte enhancer factor 2 *(mef2)-Gal4 line* (*mef2>*) as a driver for *darhgef10* expression in the muscle, using *pTw::darhgef10/mef2-Gal4* flies. As *mef2* is a transcription factor that is necessary for embryonic muscle development and is expressed in the developing heart (Lilly *et al.*, 1995; Gajewski *et al.*, 1997). However, the *mef2>arhgef10* combination produces a rounded muscle phenotype (Figure 37) that leads to lethality during the L1 larval stage, preventing us to use it in an assay where we intended to find both suppressors or enhancers of *darhgef10* activity.

The rounded muscle cell phenotype produced by *mef2>darhgef10* also provides insight about dArhgef10 activity. A similar phenotype had been identified when the function of muscle attachment factors such as integrins, integrin-linked protein kinase (ILK) and Talin was reduced in large scale RNAi screens (Schnorrer *et al.*, 2010). To gain confidence on the results we obtained in the *ey>* experiments, we can develop a recombinant between *mef2* and *darhgef10* by using a *tub-Gal80* temperature sensitive [ts] with a similar strategy used in *ey>*. This recombinant line could be maintained at 18ºC, avoiding Gal4 transcriptional activation activity, which would prevent *mef2>darhgef10*-induced lethality. We would then cross these recombinants with flies carrying mutations or RNAi against possible *darhgef10* effectors. Full suppression of the rounded muscle phenotype could lead to eclosion of adults, so it would be easily scorable. The specificity of the suppression would be confirmed directly by live imaging of F1 embryos using the *UAS-lifeact-GFP,Mef2Gal4* reporter line. Just as an example, live imaging of embryos carrying *mef2>arhgef10* and *>lifeact-GFP* is shown in Figure IV of the annexes.

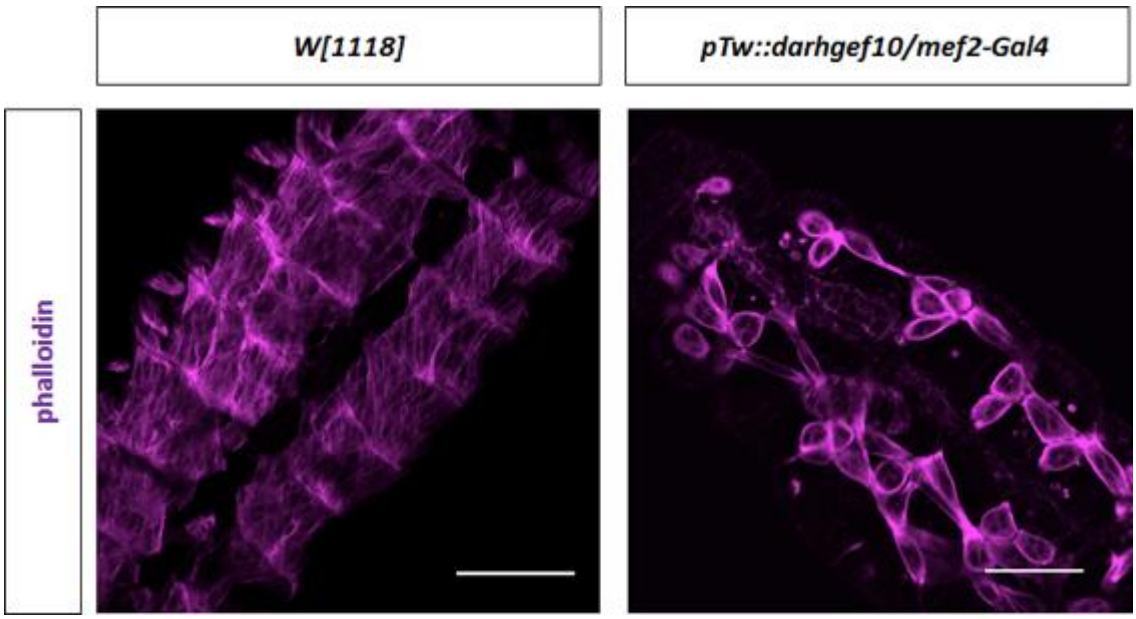

Figure 37 – Confocal image showing body wall muscles stained with phalloidin in *w[1118]* and *mef2>darhgef10* (*pTW::darhgef10/mef2-Gal4*) stage 16 embryos. The rounded muscle phenotype is noticeable in *mef2>darhgef10* embryos (Right panels). Scale bar: 50 µm.

Chapter 4. Conclusion

Homozygous mutants for the *darhgef10* gene have a congenital heart defect consisting of misaligned cardiac cells, yet they are viable and fertile. Before this thesis work, the molecular pathways and cellular processes that malfunction in the absence of *darhgef10*, resulting in the congenital heart defect, were not known. It was also unclear whether the cardiac defect of *darhgef10* mutants was associated with any lethality or compromised life history trait. As the human homolog of *darhgef10, ARHGEF10*, is expressed in the heart and has been previously linked to cardiovascular disease, we set out to characterize the development and adult life history traits of *darhgef10* mutants and in parallel developed novel tools and assays to learn more about dArhgef10 biology and begin to investigate the cellular basis of the heart defect.

We have determined that approximately 50% of *darhgef10* mutants die during development. Surprisingly, the surviving *darghef10* mutant flies have a rather normal or even slightly improved lifespan and locomotor performance as adults relative to control flies. In contrast, ectopic expression of *darhgef10* in muscle leads to L1 stage lethality with an associated rounded body muscle phenotype. Ectopic overexpression in other developing tissues such as the salivary gland and the eye imaginal disc also causes severe morphological defects, enabling us to conclude that high levels of dArhgef10 is highly disruptive to tissue morphogenesis. We have also provided molecular and genetic evidence that dArhgef10 might achieve these activities by associating with F-actin accumulations and stimulating ROCK-like Rho-kinase (Rok) activity. This work significantly advances both our understanding about how dArhgef10 functions and the consequences of not having *darhgef10* during development and adult life. Further work is required to fully understand the role of *darhgef10* during heart development.

In the future we intend to further investigate the role of Rok as a dArhgef10 effector. If Rok is indeed necessary for dArhgef10 activity, it is expected that reduced Rok activity in the heart would also lead to a misaligned cardioblasts phenotype. In parallel, we will continue our efforts to define the subcellular localization of endogenous dArhgef10 with a new CRISPR-Cas9 approach. Since *darhgef10* deletion does not seem to affect the behavior of adult flies, it will be interesting to check the adult heart to conclude if the defect is maintained in the adult or if it is, for instance, improved after metamorphosis remodeling.

Chapter 5. Bibliography

AOKI, Takuji *et al.* - Regulation of mitotic spindle formation by the RhoA guanine nucleotide exchange factor ARHGEF10. **BMC cell biology**. ISSN 1471-2121. 10 (2009) 56.

ASHBURNER, Michael; ROOTE, John - Maintenance of a Drosophila laboratory: general procedures. **CSH protocols**. ISSN 1932-6203. 2007, 6 (2007)

BIER, Ethan; BODMER, Rolf - Drosophila, an emerging model for cardiac disease. **Gene**. ISSN 0378-1119, 342 (2004) 1–11.

BISHOP, Anne L.; HALL, Alan - Rho GTPases and their effector proteins. **Biochemical Journal**. ISSN 0264-6021, 348 (2000) 241.

BODMER, Rolf; VENKATESH, Tyamagondlu V. - Heart development in Drosophila and vertebrates: Conservation of molecular mechanisms. **Developmental Genetics**. ISSN 0192-253X, 22 (1998) 181–186.

BOS, Jl; REHMANN, Holger; WITTINGHOFER, Alfred - GEFs and GAPs : Critical Elements in the Control of Small G Proteins. **Cell**. . ISSN 0092-8674 (2007) 865–877.

BRYANTSEV, Anton L.; CRIPPS, Richard M. - Cardiac gene regulatory networks in Drosophila. **Biochimica et Biophysica Acta - Gene Regulatory Mechanisms**. ISSN 1874-9399. 1789, 4 (2009) 343–353.

CHAYA, Taro *et al.* - Identification of a negative regulatory region for the exchange activity and characterization of T332I mutant of Rho guanine nucleotide exchange factor 10 (ARHGEF10). **Journal of Biological Chemistry**. ISSN 0021-9258. 286, 34 (2011) 29511–29520.

CHERFILS, Jacqueline; ZEGHOUF, Mahel - Regulation of small GTPases by GEFs, GAPs, and GDIs. **Physiological reviews**. ISSN 1522-1210, 93 (2013) 269–309.

CÔTÉ, Jean François; VUORI, Kristiina - GEF what? Dock180 and related proteins help Rac to polarize cells in new ways. **Trends in Cell Biology**. ISSN 0962-8924. 17, 8 (2007) 383–393.

CÔTÉ, Jean-François *et al.* - A novel and evolutionarily conserved PtdIns(3,4,5)P3-binding domain is necessary for DOCK180 signalling. **Nature cell biology**. ISSN 1465-7392. 7, 8 (2005) 797–807.

CRIPPS, Richard M.; OLSON, Eric N. - Control of cardiac development by an evolutionarily conserved transcriptional network. **Developmental biology**. ISSN 0012-1606. 246 (2002) 14–28.

DIETZL, Georg *et al.* - A genome-wide transgenic RNAi library for conditional gene inactivation in Drosophila. **Nature**. ISSN 0028-0836. 448, July (2007) 151–156.

EKENSTEDT, Kari J. *et al.* - An ARHGEF10 Deletion Is Highly Associated with a Juvenile-Onset Inherited Polyneuropathy in Leonberger and Saint Bernard Dogs. **PLoS Genetics**. ISSN 1553-7404. 10, 10 (2014) e1004635.

ETIENNE-MANNEVILLE, Sandrine; HALL, Alan - Rho GTPases in cell biology. **Nature**. ISSN 0028-0836. 420, December (2002) 629–635.

FAHED, Akl C. *et al.* - Genetics of congenital heart disease: The glass half empty. **Circulation Research**. ISSN 0009-7330. 112 (2013) 707–720.

FEHON, Richard G.; MCCLATCHEY, Andrea I.; BRETSCHER, Anthony - Organizing the cell cortex: the role of ERM proteins. **Nature reviews. Molecular cell biology**. ISSN 1471-0072. 11, ApRIl (2010) 276–287.

GAJEWSKI, Kathleen *et al.* - D-mef2 is a target for Tinman activation during Drosophila heart development. **EMBO Journal**. ISSN 0261-4189. 16, 3 (1997) 515–522.

GARCÍA-MATA, Rafael; BURRIDGE, Keith - Catching a GEF by its tail. **Trends in Cell Biology**. ISSN 0962-8924. 17, 1 (2007) 36–43.

GELB, Bruce D.; CHUNG, Wendy K. - Complex Genetics and the Etiology of Human Congenital Heart Disease. **Cold Spring Harbor perspectives in medicine**. ISSN 2157-1422. 4, (2014).

GOICOECHEA, Silvia M. *et al.* - I'm coming to GEF you: Regulation of RhoGEFs during cell migration. **Cell adhesion & migration**. ISSN 1933-6926. 8, (2014) 1–15.

HALSELL, Susan R.; CHU, Benjamin I.; KIEHART, Daniel P. - Genetic analysis demonstrates a direct link between Rho signaling and nonmuscle myosin function during Drosophila morphogenesis. **Genetics**. ISSN 0016-6731. 155 (2000) 1253–1265.

HAN, Zhe *et al.* - Hand, an evolutionarily conserved bHLH transcription factor required for Drosophila cardiogenesis and hematopoiesis. **Development (Cambridge, England)**. ISSN 0950-1991. 133 (2006) 1175–1182.

HAN, Zhe; BODMER, Rolf - Myogenic cells fates are antagonized by Notch only in asymmetric lineages of the Drosophila heart, with or without cell division. **Development (Cambridge, England)**. ISSN 0950-1991. 130 (2003) 3039–3051.

HARTENSTEIN, A Y. *et al.* - The function of the neurogenic genes during epithelial development in the Drosophila embryo. **Development (Cambridge, England)**. ISSN 0950-1991. 116, (1992) 1203–1220.

HEASMAN, Sarah J.; RIDLEY, Anne J. - Mammalian Rho GTPases: new insights into their functions from in vivo studies. **Nature reviews. Molecular cell biology**. ISSN 1471-0072. 9, SEPTEMBER (2008) 690–701.

HOFFMAN, Julien I. ..; KAPLAN, Samuel - The incidence of congenital heart disease. **Journal of the American College of Cardiology**. ISSN 0735-1097. 39, 12 (2002) 1890–1900.

HOLLFELDER, Dominik; FRASCH, Manfred; REIM, Ingolf - Distinct functions of the laminin β LN domain and collagen IV during cardiac extracellular matrix formation and stabilization of alary muscle attachments revealed by EMS mutagenesis in Drosophila. **BMC developmental biology**. ISSN 1471-213X. 14, 1 (2014) 26.

J.I.E., Hoffman - The global burden of congenital heart disease. **Cardiovascular Journal of Africa**. ISSN 1680-0745. 24, 4 (2013) 141–145.

JINEK, M. *et al.* - A Programmable Dual-RNA-Guided DNA Endonuclease in Adaptive Bacterial Immunity. **Science**. ISSN 0036-8075. 337, June (2012) 816–821.

LILLY, B. *et al.* - Requirement of MADS domain transcription factor D-MEF2 for muscle formation in Drosophila. **Science (New York, N.Y.)**. ISSN 0036-8075. 267, February (1995) 688–693.

MAGIE, Craig R.; PARKHURST, Susan M. - Rho1 regulates signaling events required for proper Drosophila embryonic development. **Developmental Biology**. ISSN 0012-1606. 278 (2005) 144–154.

Mantas Dias, Ângela- CG43658 is a novel RhoGEF required for Drosophila melanogaster heart formation. Lisboa: Instituto de Medicina Molecular, 2012. Tese de Mestrado.

MARELLI, Ariane J. *et al.* - Congenital heart disease in the general population: Changing prevalence and age distribution. **Circulation**. ISSN 0009-7322. 115 (2007) 163–172.

MASON, I. J. - The ins and outs of fibroblast growth factors. **Cell**. ISSN 0092-8674. 78 (1994) 547–552.

MATSUSHITA, Tomonaga *et al.* - Functional SNP of ARHGEF10 confers risk of atherothrombotic stroke. **Human Molecular Genetics**. ISSN 0964-6906. 19, 6 (2010) 1137–1146.

MATTILA, Pieta K.; LAPPALAINEN, Pekka - Filopodia: molecular architecture and cellular functions. **Nature reviews. Molecular cell biology**.ISSN 1471-0072. 9, june (2008) 446–454.

MEDIONI, Caroline *et al.* - The fabulous destiny of the Drosophila heart. **Current Opinion in Genetics and Development**. ISSN 0959-437X. 19 (2009) 518–525.

MELLER, Nahum; MERLOT, Sylvain; GUDA, Chittibabu - CZH proteins: a new family of Rho-GEFs. **Journal of cell science**. ISSN 0021-9533. 118 (2005) 4937–4946.

MOHL, M. *et al.* - Gef10 - The third member of a Rho-specific guanine nucleotide exchange factor subfamily with unusual protein architecture. **Naunyn-Schmiedeberg's Archives of Pharmacology**. ISSN 0028-1298. 373 (2006) 333–341.

MOLINA, Marco R.; CRIPPS, Richard M. - Ostia, the inflow tracts of the Drosophila heart, develop from a genetically distinct subset of cardial cells. **Mechanisms of Development**. ISSN 0925-4773. 109 (2001) 51–59.

MURALI, Arun; RAJALINGAM, Krishnaraj - Small Rho GTPases in the control of cell shape and mobility. **Cellular and Molecular Life Sciences**. ISSN 1420-9071. 71 (2014) 1703–1721.

NI, Jian-Quan *et al.* - Vector and parameters for targeted transgenic RNA interference in Drosophila melanogaster. **Nature methods**. ISSN 1548-7091. 5, December (2008) 49–51.

NICHOLS, Charles D.; BECNEL, Jaime; PANDEY, Udai B. - Methods to Assay *Drosophila* Behavior. **Journal of Visualized Experiments**. ISSN 1940-087X (Electronic). March (2012) 3–7.

PAREYSON, Davide - Charcot-Marie-Tooth disease and related neuropathies: Molecular basis for distinction and diagnosis. **Muscle and Nerve**. ISSN 0148-639X. 22, November (1999) 1498–1509.

PARK, M. *et al.* - The wingless signaling pathway is directly involved in Drosophila heart development. **Developmental biology**. ISSN 0012-1606. 177, 0149 (1996) 104–116.

PARK, Maiyon; VENKATESH, Tyamagondlu V.; BODMER, Rolf - Dual role for the zeste-white3/shaggy-encoded kinase in mesoderm and heart development of Drosophila. **Developmental Genetics**. ISSN 0192-253X. 22 (1998) 201–211.

PARKS, Annette L. *et al.* - Systematic generation of high-resolution deletion coverage of the Drosophila melanogaster genome. **Nature genetics**. ISSN 1061-4036. 36, 3 (2004) 288–292.

PERTZ, Olivier - Spatio-temporal Rho GTPase signaling - where are we now? **Journal of cell science**. ISSN 0021-9533. 123 (2010) 1841–1850.

PILAURI, Vepkhia *et al.* - Gal80 dimerization and the yeast GAL gene switch. **Genetics**. ISSN 0016-6731. 169, April (2005) 1903–1914.

PONZIELLI, Romina *et al.* - Heart tube patterning in Drosophila requires integration of axial and segmental information provided by the Bithorax Complex genes and hedgehog signaling. **Development (Cambridge, England)**. ISSN 0950-1991. 129 (2002) 4509–4521.

PORT, Fillip *et al.* - Optimized CRISPR/Cas tools for efficient germline and somatic genome engineering in Drosophila. **Proceedings of the National Academy of Sciences of the United States of America**. ISSN 1091-6490. (2014) E2967–E2076.

QUIRING, R. *et al.* - Homology of the eyeless gene of Drosophila to the Small eye gene in mice and Aniridia in humans. **Science (New York, N.Y.)**. ISSN 0036-8075. 265, August (1994) 785–789.

RELLER, Mark D. *et al.* - Prevalence of Congenital Heart Defects in Metropolitan Atlanta, 1998-2005. **Journal of Pediatrics**. ISSN 0022-3476. 153 (2008) 807–813.

RIDLEY, A J. - Rho GTPases in cell migration. **J. Cell Sci.** ISSN 2154-1256. 114, (2001) 2713–2722.

ROSSMAN, Kent L.; DER, Channing J.; SONDEK, John - GEF means go: turning on RHO GTPases with guanine nucleotide-exchange factors. **Nature reviews. Molecular cell biology**. ISSN 1471-0072. 6 (2005) 167–180.

SADOK, Amine; MARSHALL, Chris J. - Rho GTPases: masters of cell migration. **Small GTPases**. ISSN 2154-1256. 5, (2014) e29710.

SCHINDELIN, Johannes *et al.* - Fiji: an open-source platform for biological-image analysis. **Nature Methods**. ISSN 1548-7091. 9, 7 (2012) 676–682.

SCHMIDT, Anja; HALL, Alan - Guanine nucleotide exchange factors for Rho GTPases : turning on the switch. **Genes & Development**. ISSN 0890-9369. (2002) 1587–1609.

SCHNORRER, Frank *et al.* - Systematic genetic analysis of muscle morphogenesis and function in Drosophila. **Nature**. ISSN 0028-0836. 464 (2010) 287–291.

SHIMOKAWA, Hiroaki; TAKESHITA, Akira - Rho-kinase is an important therapeutic target in cardiovascular medicine. **Arteriosclerosis, Thrombosis, and Vascular Biology**. ISSN 1079-5642. 25 (2005) 1767–1775.

SIT, Soon-Tuck; MANSER, Ed - Rho GTPases and their role in organizing the actin cytoskeleton. **Journal of cell science**. ISSN 0021-9533. 124 (2011) 679–683.

TAO, Ye; SCHULZ, Robert A - Heart development in Drosophila. **Seminars in cell & developmental biology**. ISSN 1084-9521. 18 (2007) 3–15.

VERHOEVEN, Kristien *et al.* - Slowed conduction and thin myelination of peripheral nerves associated with mutant rho Guanine-nucleotide exchange factor 10. **American journal of human genetics**. ISSN 0002-9297. 73 (2003) 926–932.

VOGLER, Georg; BODMER, Rolf - Cellular Mechanisms of Drosophila Heart Morphogenesis. **Journal of Cardiovascular Development and Disease**. ISSN 2308-3425. 2 (2015) 2–16.

WINTER, Christopher G. *et al.* - Drosophila Rho-associated kinase (Drok) links Frizzled-mediated planar cell polarity signaling to the actin cytoskeleton. **Cell**. ISSN 0092-8674. 105 (2001) 81–91.

WU, J. S.; LUO, L. - A protocol for mosaic analysis with a repressible cell marker (MARCM) in Drosophila. **Nat Protoc**. ISSN 1750-2799. 1, 6 (2006) 2583–2589.

WU, X.; GOLDEN, K.; BODMER, R. - Heart development in Drosophila requires the segment polarity gene wingless. **Developmental biology**. ISSN 0012-1606. 169 (1995) 619–628.

YIN, Yan-Ying *et al.* - The functional SNP rs4376531 in the ARHGEF gene is a risk factor for the atherothrombotic stroke in Han Chinese. **Neurology India**. ISSN 0028-3886. 59 (2011) 408–412.

ZAFFRAN, Stéphane *et al.* - Cardioblast-intrinsic Tinman activity controls proper diversification and differentiation of myocardial cells in Drosophila. **Development (Cambridge, England)**. ISSN 0950-1991. 133 (2006) 4073–4083.

ZAFFRAN, Stéphane; FRASCH, Manfred - Early signals in cardiac development. **Circulation Research**. ISSN 0009-7330. 91 (2002) 457–469.

ZHANG, Fujian *et al.* - Cubilin and amnionless mediate protein reabsorption in Drosophila nephrocytes. **Journal of the American Society of Nephrology : JASN**. ISSN 1533-3450. 24 (2013) 209–16.

Annexes

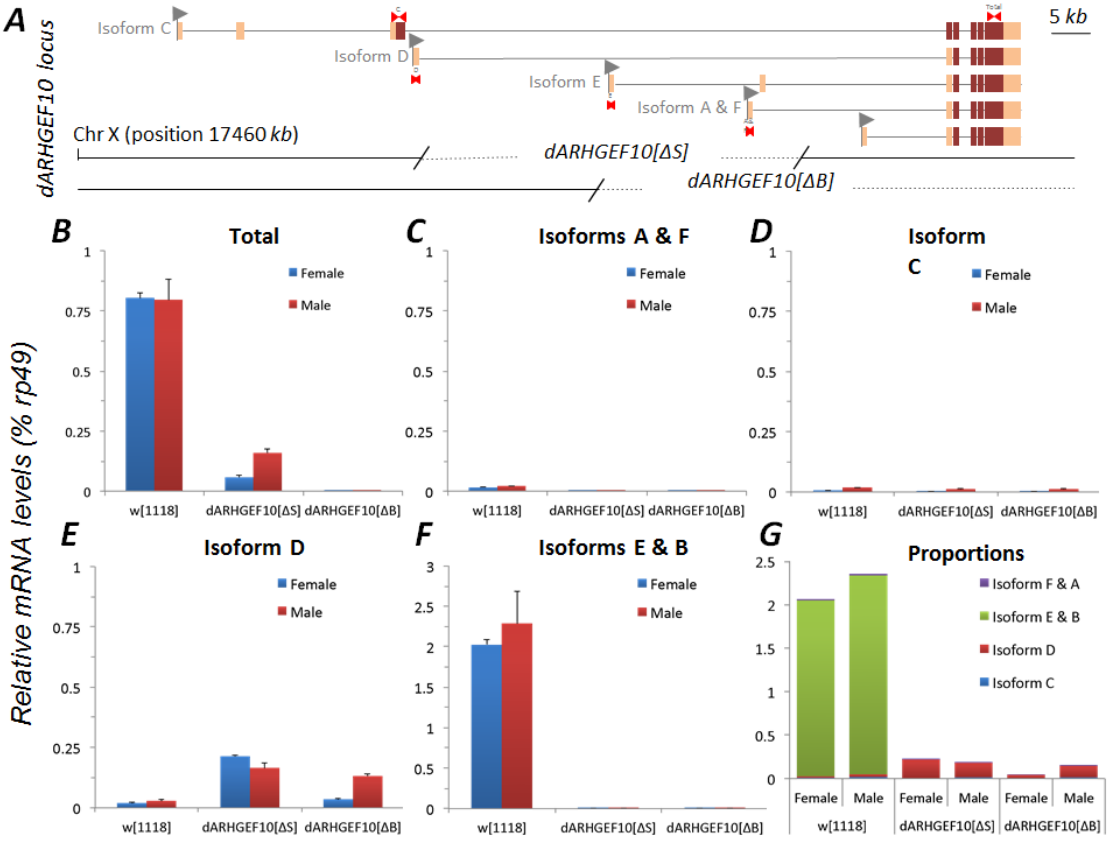

Figure I – Relative levels of *darhgef10* transcript in *darhgef10* mutants (Heredia, Mantas Dias and Gontijo, unpublished results).

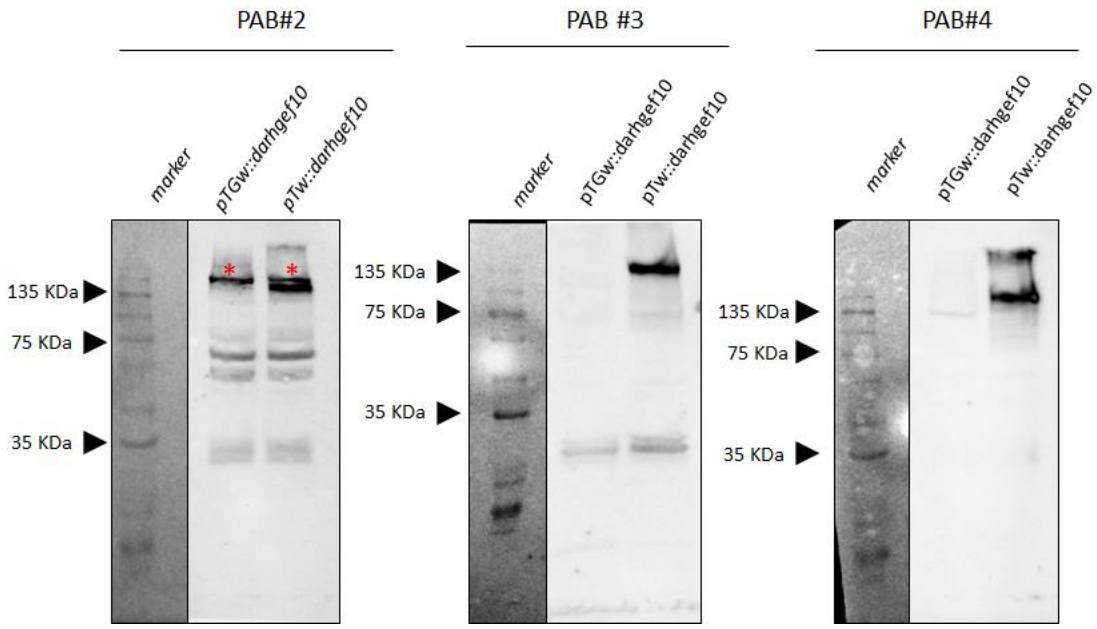

Figure II – dArhgef10 detection by Western blot using lysates of S2 cells transfected with *pTGw::darhgef10,* which leads to GFP::dArhgef10 overexpression, and *pTw::darhgef10* which leads to the overexpression of untagged dArhgef10. All cells were co-transfected with the Act-Gal4 plasmid. The four anti-dArhgef10 PABs were tested. PAB#1 did not produce any detectable band (not shown). Red asterisks indicate unspecific band close to dArhgef10 expected molecular weight band.

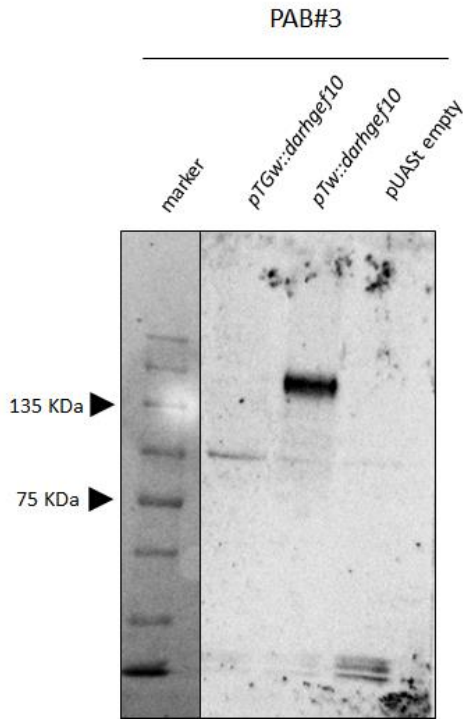

Figure III – Full membrane of Western blot analysis of *darhgef10* overexpression in S2 cells transfected with a *pTGw::darhgef10* plasmid for overexpression of *darhgef10* marked with GFP, with a *pTw::darhgef10* plasmid for overexpression of untagged *darhgef10* and with a *pUAST*-empty plasmid to serve as a control.

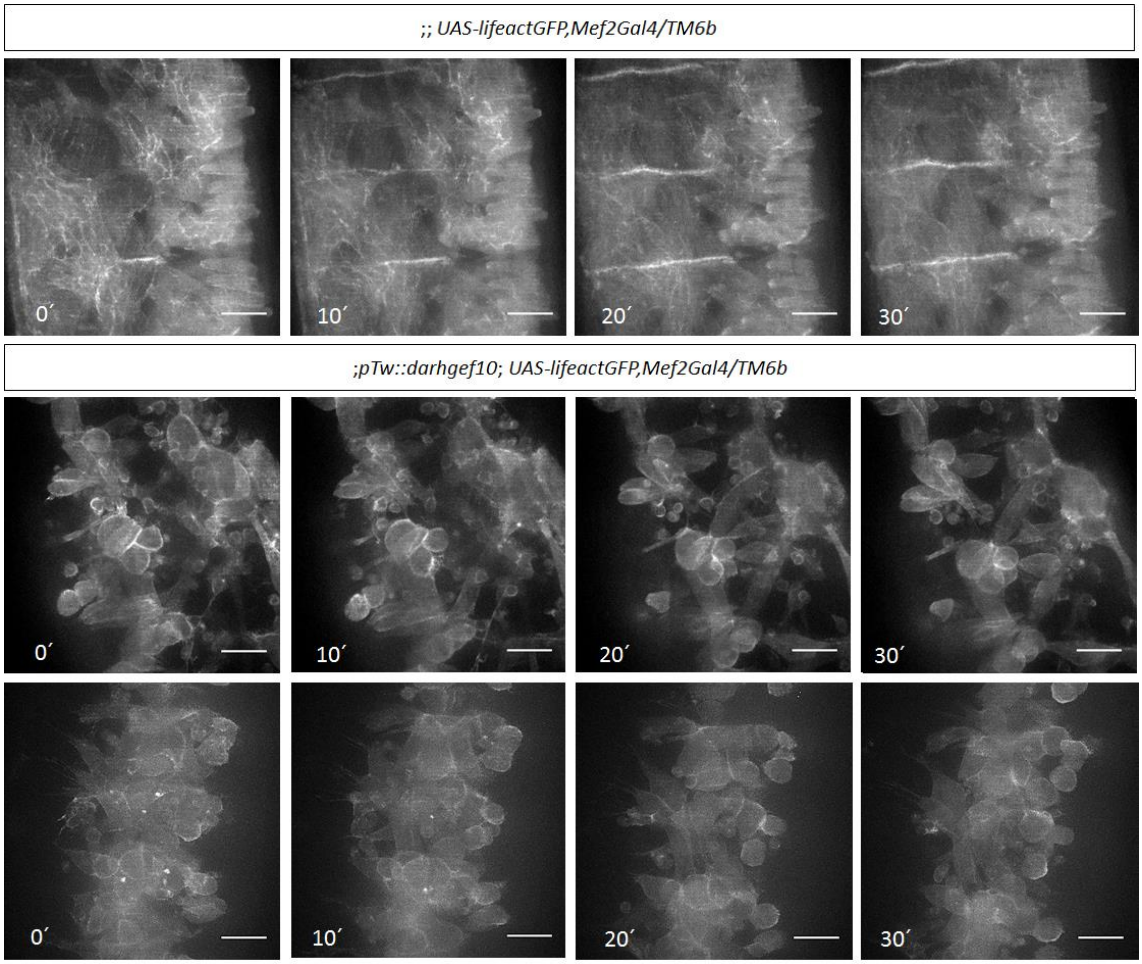

Figure IV – Projection of z-stacks of spinning disc imaging. Live imaging of muscle development in gain of function mutant embryos (bottom) and control embryos (top), using a lifeact-GFP reporter. Scale bars: 20 µm.